Triaryl-1,3,5-triazinane-2,4,6-triones (Isocyanurates) Peripherally Functionalized by Donor Groups: Synthesis and Study of Their Linear and Nonlinear Optical Properties

ARTICLE *in* CHEMISTRY - A EUROPEAN JOURNAL · SEPTEMBER 2012

Impact Factor: 5.73 · DOI: 10.1002/chem.201200484 · Source: PubMed

CHEMISTRY
A EUROPEAN JOURNAL

FULL PAPER

DOI: 10.1002/chem.201200484

Triaryl-1,3,5-triazinane-2,4,6-triones (Isocyanurates) Peripherally Functionalized by Donor Groups: Synthesis and Study of Their Linear and Nonlinear Optical Properties

Gilles Argouarch,[a] Romain Veillard,[a] Thierry Roisnel,[a] Anissa Amar,[a, b] Hacène Meghezzi,[b] Abdou Boucekkine,*[a] Vincent Hugues,[c, d] Olivier Mongin,[a, c] Mireille Blanchard-Desce,*[c, d] and Frédéric Paul*[a]

Abstract: The linear optical (LO) and nonlinear optical (NLO) properties of a series of isocyanurates functionalized by donor arms at the periphery are reported herein. These octupolar derivatives were obtained in a straightforward way from commercial isocyanate derivatives and were fully characterized. Although several of these compounds are known, those that exhibited the largest NLO activities are all new compounds. In terms of second-order activity, several of these derivatives exhibit remarkable activity/transparency tradeoffs. In terms of third-order activity, the longer derivatives with the stronger donor groups ($X=NH_2$, NMe_2, or NPh_2) were shown to possess significant two-photon absorption cross sections. These strongly luminescent derivatives exhibit two-photon absorption cross sections up to 410 GM. DFT computations were also conducted to unravel their electronic structures and to rationalize their NLO properties. To our knowledge, the present study is the first concerned with the nonlinear optical properties of these original cyclotrimers.

Keywords: density functional calculations · isocyanurates · nonlinear optics · synthetic methods · two-photon absorbers

Introduction

Triazinane-2,4,6-triones, more commonly known as isocyanurates (**A**; Scheme 1), are cyclotrimeric molecules that have attracted considerable attention in polymer chemistry in regard to their numerous industrial applications,[1] particularly in the field of foams, elastomers, paints, fibers, and surface coatings.[2] Thus, when used as cross-linking groups between polyurethane-based strands, isocyanurate units allow enhancement of the flame resistance, thermal stability, and rigidity of the resulting polymers.[1b,3] Alternatively, as discrete molecules, they also intervene as key precursors in important industrial processes concerned with the synthesis of several polyurethane copolymers, but also as activators in the polymerization of ε-caprolactam.[4] As reactants or additives, these chemicals are often very attractive from an atom-economy perspective because most of them can be obtained in good yields and in a single step from the corresponding isocyanate monomers by the use of specific catalysts.[5] Also, after proper functionalization, they have also given rise to more original applications, such as chloride anion receptors,[6] drug-delivery agents,[7] or tensioactive building blocks.[8]

However, up to now, these symmetric units had attracted only scant attention for their (nonlinear) optical properties.[9] This lack of interest is surprising because, owing to their planar D_{3h} or twisted pseudo-D_3 symmetry (**A**; Scheme 1), these compounds might exhibit significant second-[10] and third-order[11] nonlinear optical (NLO) activities when the central electron-attracting isocyanurate core is symmetrically decorated with electron-releasing arms, likewise to related structures based on 1,3,5- and 2,4,6-substituted phenyl derivatives (**B**; Scheme 1).[12] In accordance with the first expectation, we have recently shown by hyper Rayleigh scattering (HRS) that derivatives such as **1-X** and **2-X**

[a] Dr. G. Argouarch, R. Veillard, Dr. T. Roisnel, A. Amar, Prof. A. Boucekkine, Dr. O. Mongin, Dr. F. Paul
Sciences Chimiques de Rennes, CNRS (UMR 6226)
Université de Rennes 1, Campus de Beaulieu
35042 Rennes Cedex (France)
Fax: (+33) 02-23-23-69-39
E-mail: abdou.boucekkine@univ-rennes1.fr
frederic.paul@univ-rennes1.fr

[b] A. Amar, Prof. H. Meghezzi
Laboratoire de Thermodynamique et Modélisation Moléculaire
USTHB
BP 32, El Alia, 16111
Bab Ezzouar Alger (Algeria)

[c] V. Hugues, Dr. O. Mongin, Dr. M. Blanchard-Desce
Chimie et Photonique Moléculaires, CNRS (UMR 6510)
Université de Rennes 1, Campus de Beaulieu
35042 Rennes Cedex (France)

[d] V. Hugues, Dr. M. Blanchard-Desce
ISM, CNRS (UMR 5255)
Université Bordeaux
33400 Talence France
Fax: (+33) 05-40-00-67-35
E-mail: mireille.blanchard-desce@u-bordeaux1.fr

Supporting information for this article is available on the WWW under http://dx.doi.org/10.1002/chem.201200484.

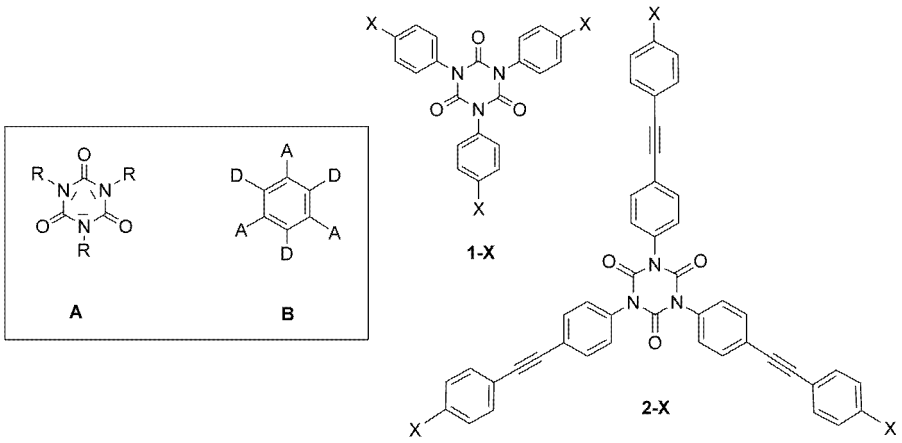

Scheme 1. The isocyanurate core (with the nonbonding doublets on the nitrogen atoms explicitly drawn) versus the octupolar D_{3h} phenyl derivatives (insert) and the target molecules. A = electron-withdrawing groups, D = electron-releasing groups.[13]

(X = OMe, NMe_2) possess remarkable hyperpolarizabilities.[14] Given that such octupolar structures might also present good activities for specific third-order NLO properties, such as two-photon absorption (TPA),[11] we have now completed our previous report on these compounds[14] by studying their luminescence and have subsequently used their luminescence to determine the TPA cross sections of selected derivatives. Although the synthesis of some of these cyclotrimers has been briefly reported, a more complete account of their synthesis is now disclosed. The experimental work has also been complemented by DFT calculations. Such calculations were useful to obtain insight into the origin of the NLO properties of these octupolar compounds.

Results

Synthesis and characterization: Although *para*-functional arylisocyanurates **1-X** that feature electron-releasing X substituents (X = OMe, NH_2, NMe_2) at the periphery were initially targeted for their second-order NLO properties,[14] some derivatives that feature strongly electron-attracting substituents, *para*-functional arylisocyanurates **1-X** (X = NO_2, CN), were also targeted to complete our experimental data on these compounds. The synthesis of most of these arylisocyanurates (X = NO_2, CN Br, OMe, NMe_2) was achieved by directly cyclotrimerizing the corresponding isocyanates, when commercially available [Scheme 2, Eq. (1)]. Several organic or inorganic efficient catalysts have been reported for this reaction.[2g,5,15] We used cesium fluoride as a catalyst to carry out the trimerization because it is commercially available and relatively cheap.[16] With this catalyst, good yields of most of the desired isocyanurates could be obtained in one step after chromatographic purification. Notably, the use of nitrobenzene as a solvent allows the medium to remain fluid during all the reaction, and even perfectly homogeneous in most cases. In that respect, our procedure contrasts with that previously reported by Nambu and Endo, which was solvent-free and thus only applicable to liquid isocyanates.[16] Even in the case of **1-NO_2** or **1-CN**, for which the workup was complicated by the low solubility, this experimental procedure permitted us to achieve high conversions of isocyanates into the corresponding isocyanurates. In contrast to the other **1-X** derivatives, the amino compound **1-NH_2** was not isolated directly from the isocyanate precursor, but in a subsequent reaction of a Clemmensen-type reduction of the nitro cyclotrimer **1-NO_2** [Scheme 2, Eq. (2)]. Most of the **1-X** derivatives have been previously reported, but were not always extensively characterized.[17] Thus, all **1-X** derivatives isolated have now been fully characterized by usual spectroscopic analysis (i.e., IR, Raman, and NMR spectroscopies). Mass spectrometric or/and elemental analysis were performed on the new derivatives **1-CN** and **1-NH_2**.

All these compounds show a diagnostic AA′BB′ pattern in the ^{1}H NMR spectra for the functional peripheral rings. The presence of carbonyl groups is evidenced by the occurrence of a signal near $\delta = 150$ ppm in the ^{13}C NMR spectra.

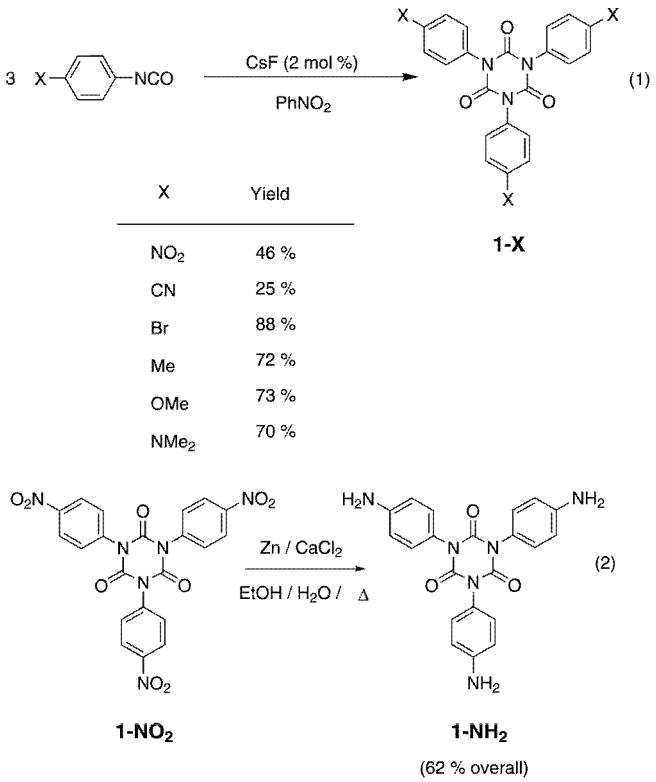

Scheme 2. Synthesis of cyclotrimers **1-X**.

A very strong absorption is also observed near $\tilde{\nu}=1710\,cm^{-1}$ in the IR spectra, which can be attributed to one of the ν_{CO} stretching modes of the three carbonyl groups. This ν_{CO} mode is not visible in the Raman spectra. Instead, a moderate-to-intense Stokes band, which also corresponds to a very weakly absorbing mode in the IR spectra, is present near $\tilde{\nu}=1770\,cm^{-1}$. On the basis of the vibrational selection rules applied to D_3 or C_3 molecules, the symmetric ν_{CO} stretch that belongs to A-type irreducible representations should be essentially active in the Raman spectra, whereas that that belongs to E-type representations should be active in the IR spectra and also weakly in the Raman spectra.[19] In contrast to these predictions, we detected two modes in the IR spectra and only one in the Raman spectra. However, one of the IR active ν_{CO} modes appears to be much weaker than the other. Thus, we propose that the weak mode at higher energy in the IR spectra corresponds to the symmetric (A-type) ν_{CO} stretching mode, whereas the other, much more intense, would correspond to the nonsymmetric ν_{CO} stretching mode (E-type). Beside these intensity-related considerations, this attribution is also supported by our DFT calculations (see later).

We next attempted to isolate longer homologues bearing electron-releasing substituents by using standard Sonogashira coupling protocols. Two synthetic routes were envisioned (Scheme 3): either by 1) treating the tris-bromo cyclotrimer **1-Br** with functional aryl alkynes (route A) or 2) treating a tris-alkyne cyclotrimer **3-H** with functional aryl iodides (route B). We decided to test both of these routes by using the methoxy group (X=OMe) as a model compound. Both synthetic routes required a Sonogashira coupling step with **1-Br** (Scheme 4). The poor solubility of this cyclotrimer renders the coupling sluggish in usual organic solvents. The reaction has therefore to be performed in DMF under rather harsh conditions to isolate any of these tris-coupled products (**3-TMS** or **2-OMe**) in satisfactory yields.

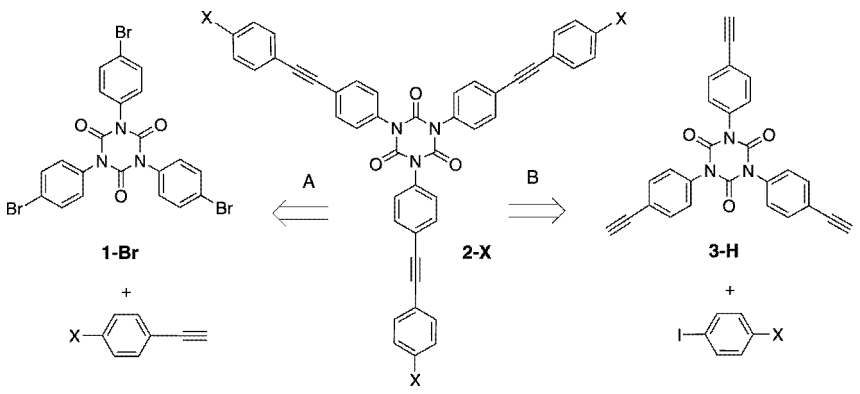

Scheme 3. Synthetic routes envisioned to access the extended cyclotrimers **2-X**.

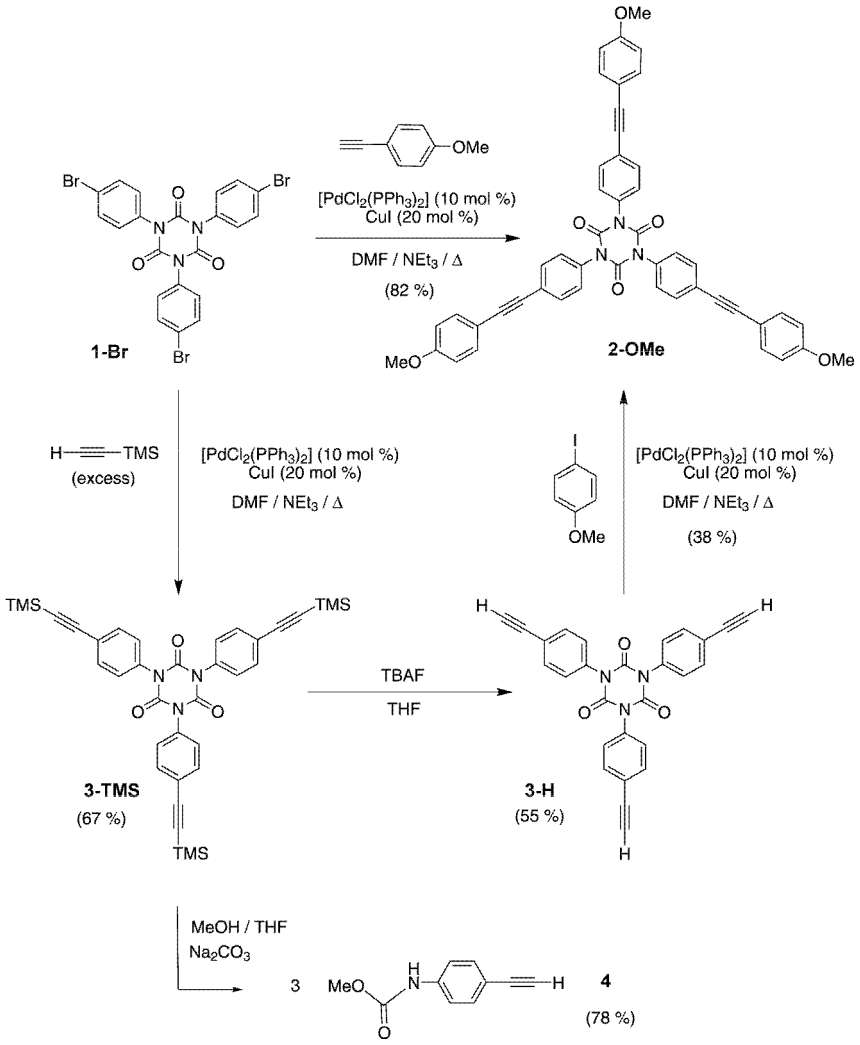

Scheme 4. Comparison of the synthetic routes A and B to obtain **2-OMe**. TBAF = tetrabutylammonium fluoride. TMS = trimethylsilyl.

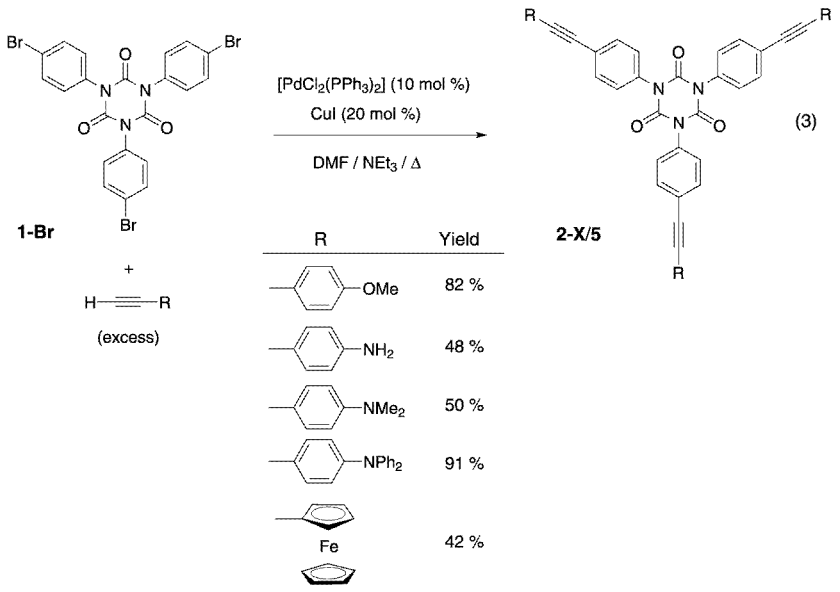

Scheme 5. Synthesis of the extended cyclotrimers **2-X** and **5**.

Route A proved attractive to access the **2-X** compounds because **2-OMe** was obtained in 82% after one step from **1-Br** and *para*-ethynyl anisole (Scheme 4). We had to isolate **3-H** first to test route B, which was carried out in two steps (Scheme 4). First, the TMS-protected compound **3-TMS** was isolated from **1-Br** by using a Sonogashira coupling. The desilylation of **3-TMS** was next attempted with sodium carbonate. Much to our surprise, essentially the corresponding carbamate **4** could be isolated (78%). Quite likely, under these conditions, ring opening of the cyclotrimer **3-TMS** takes place simultaneously with deprotection and the alkynyl carbamate **4** is formed in fair yields. The latter is a new product, which was completely characterized by mass-spectrometric, the usual spectroscopic (IR, Raman, and NMR), and elemental analysis and X-ray diffraction studies (see Figure 2b). We tried to repeat the deprotection with TBAF. Under such conditions, the desired intermediate **3-H** could be isolated in fair yields (55%) and was completely characterized. The structure of this compound was also confirmed by X-ray diffraction studies (see Figure 2a). We could eventually isolate the desired compound **2-OMe** after a Sonogashira coupling with 4-iodoanisole, but the overall yield (14%) for this route was significantly lower than by the other route. Given the good synthetic access to 4-ethynyl-*N,N*-diphenylaniline[20] along with the commercial availability of the other phenylalkynyl derivatives substituted at the *para* position by donor groups, this approach was not pursued, and route A was retained as the most efficient synthetic access to the **2-X** compounds.

In a similar way to **2-OMe**, two **2-X** homologues (X = NH_2, NMe_2) were initially isolated in fair yields (Scheme 5). The very low solubility of the extended amino derivative **2-NH_2** significantly complicated its characterization, which led us to synthesize the more soluble diphenylamino derivative **2-NPh_2**.

The organometallic derivative **5** featuring ferrocenyl as a donor at each arm was also synthesized. Note that this compound had been reported in several patents, but no details about the synthesis or characterization had been given.[21] Thus, all these extended cyclotrimers were extensively characterized by the usual spectroscopic (IR, Raman, and NMR) and mass spectrometric analysis. In addition, among the new organic derivatives, **2-OMe** and **2-NMe_2** were further characterized by elemental analysis.

For the extended cyclotrimers **2-X**, the presence of the additional 1,4-phenylene unit at each arm was clearly established by the appearance of a new AA′BB′ system in the aromatic region of their ^{1}H NMR spectra. The presence of the ethynylene unit is evidenced by the presence of diagnostic ^{13}C NMR signals in the alkynyl region, near $\delta = 90$ ppm, and by a new ν_{CC} mode observed in the IR and Raman spectra, near $\delta = 2200\ cm^{-1}$. In these compounds, the symmetric (A-type) and asymmetric (E-type) alkyne stretching modes are apparently energetically degenerate (or nearly so) because only one ν_{CC} band is detected. This outcome contrasts with the ν_{CO} modes of **2-X**, for which absorptions that resemble those observed for the shorter homologues **1-X** are detected by Raman and IR spectroscopic analysis.

Solid-state structures: Isocyanurates **1-CN**, **1-Br**, and **3-H** crystallize in centrosymmetric space groups (see Figures 1a,b and 2a and the Experimental Section), which excludes any second-order NLO activity for these compounds in the crystalline state. The bond lengths and angles for these compounds appear in the usual range[22] because they compare well with those of previously characterized derivatives (see the Supporting Information), such as **1-H**,[2e,23] **1-F**,[24] **1-Cl**,[25] **1-NO_2**,[18b] and **1-*i*Pr** (Table 1).[26,27] Notably, the C=O bond lengths are slightly longer than those of typical ketones (1.19 Å), but shorter than those of typical amides (1.23 Å), whereas the (O)C=N bond lengths are significantly lower than the peripheral N–C bond lengths (ca. 1.45 Å), themselves shorter than typical single C–N bonds (1.48 Å).[22] Along with the overall planarity of the isocyanurate ring, these bonding features indicate some mesomerism between the dominating neutral valence-bond (VB) form (**A**) and the two other VB structures (**B_1** and **B_2**) in the ground state (Scheme 6), which imparts some "aromatic" character to the central ring. However, based on the bond lengths, this resonance is less pronounced in **1-X** than in typical carbamate structures such as **4**.

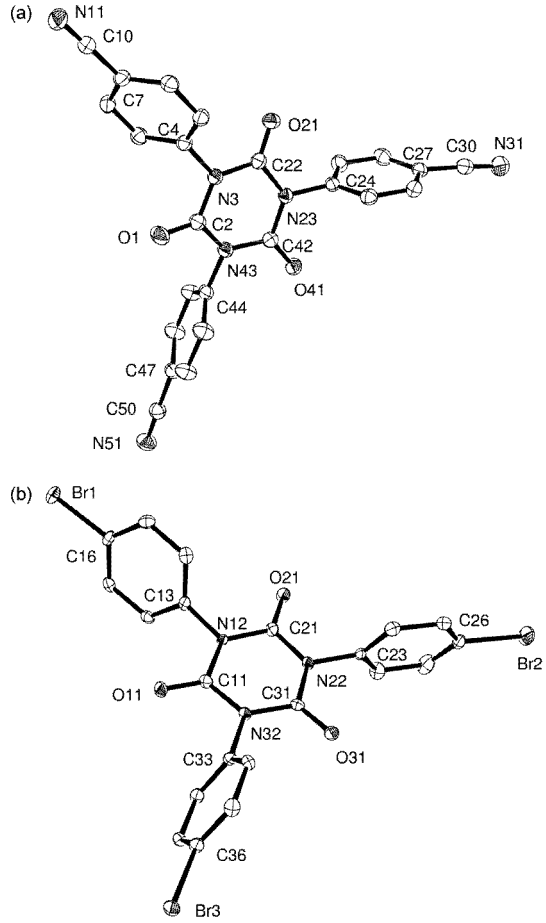

Figure 1. ORTEP representation of the complexes a) **1-CN** and b) **1-Br** at the 50% probability level. Hydrogen atoms have been omitted for clarity. Selected distances [Å]: a) C7–C10 1.447(2), C10–N11 1.147(2), C27–C30 1.448(2), C30–N31 1.146(2), C47–C50 1.4408(19), C50–N51 1.1479(19); b) C16–Br1 1.900(3), C26–Br2 1.893(3), C36–Br3 1.895(3) (also see Table 1).

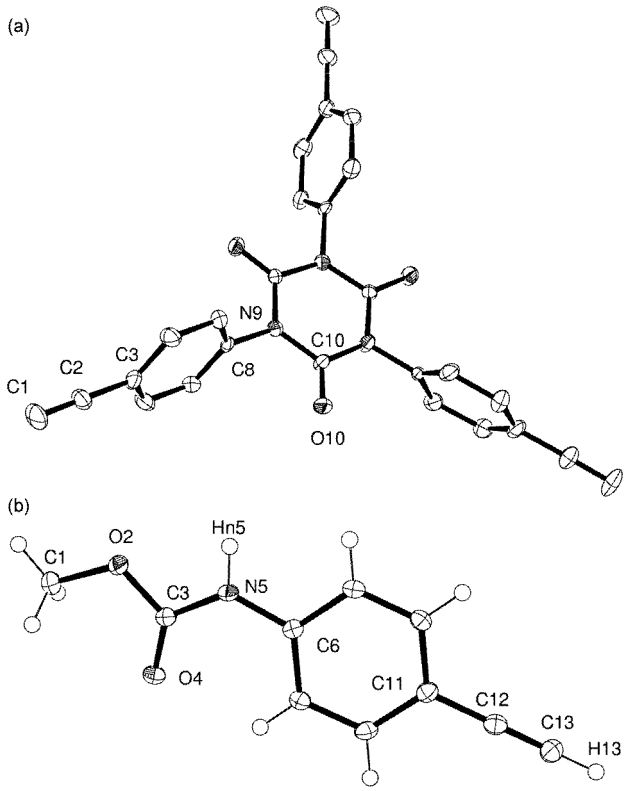

Figure 2. ORTEP representation of the complexes a) **3-H** and b) **4** at the 50% probability level. Hydrogen atoms of **3-H** have been omitted for clarity. Selected distances [Å]: a) C3–C2 1.450(6), C2–C1 1.203(6); b) C1–O2 1.4498(12), O2–C3 1.3477(12), C11–C12 1.4430(15), C12–C13 1.1946(16) (also see Table 1 for other bond lengths).

Table 1. Selected mean bond lengths and angles for the isocyanurate cores of **1-CN**, **1-Br**, **3-H**, and **4**.

Compound	**1-CN**	**1-Br**	**3-H**	**4**
Selected bond lengths [Å]				
C=O	1.204±0.001	1.205±0.008	1.206(5)	1.2195(13)
N–C(O)	1.394±0.006	1.39±0.010	1.398±0.003	1.3645(13)
C–N	1.451±0.002	1.449±0.008	1.460(5)	1.4114(13)
Selected bond angles [°]				
N-C=O	122.5±0.5	122.5(3)	122.0±0.3	126.99(10)
(O)C-N-C(O)	124.7±0.1	125.5±0.1	123.8(4)	–
N-C(O)-N	114.7±0.2	114.8±0.8	115.9(4)	–
$[(O)CN]_3/Ar$[a]	83/54/78	60/65/82	80	170

[a] Dihedral angles (±5°) between the aryl mean plane and the isocyanurate mean plane.

A close comparison between these different data sets indicates no sizeable substituent effect on the bonding distances within the isocyanurate core. This finding is understandable in all these cyclotrimers because the peripheral phenyl rings adopt a twisted conformation with dihedral angles that vary between 55 and 82° in the solid state due to the steric interactions between the *ortho*-hydrogen atoms and the three carbonyl groups of the isocyanurate core. This conformation clearly disfavors the π–π overlap and limits the electronic conjugation between the peripheral substituent on a branch and the central isocyanurate core.

In this respect, the comparison between **3-H** and **4** is instructive (Figure 2a,b) because it reveals that the phenyl ring in the latter compound prefers to remain coplanar with the

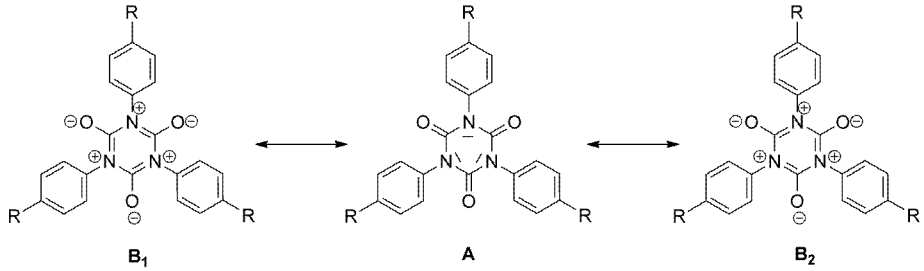

Scheme 6. Limiting VB forms of the isocyanurate ring.

-C(O)-N- fragment, when not sterically congested, to maximize π overlap. This quasi-planar conformation in **4** is certainly also somewhat stabilized by the formation of a pseudo-hydrogen bond between the carbonyl oxygen atom O4 and one of the *ortho*-hydrogen atoms on the aryl ring (H···O4: ~2.3 Å). This oxygen atom is mainly engaged in a hydrogen-bonding interaction with the amide hydrogen atom (Hn5) of a nearby molecule.[28] Such a stabilizing intermolecular interaction is clearly not observed for the cyclotrimers, which rather develop a type of pseudo-hydrogen bond[28] between one or more of their carbonyl groups and protons of nearby molecules.

One-photon absorption (OPA) studies: The linear absorption properties of isocyanurates were subsequently investigated by UV/Vis spectroscopy. Most of the **1-X** and **2-X** molecules possess a good transparency in the visible range because these compounds have their lowest lying absorption below $\lambda = 400$ nm (Table 2). As a result, the **1-X** compounds are all colorless in solution, except for the nitro compound **1-NO$_2$**, which is slightly yellowish. The lowest-lying absorption maximum of these molecules depends on the nature of the peripheral substituents and the length of the conjugated arms. The shorter cyclotrimers **1-X** that present poorly electron-withdrawing or electron-releasing substituents (i.e, Br, H, Me) have only a weak absorption that can be detected in the UV range as a shoulder above $\lambda = 250$ nm. For the more electron-withdrawing substituents (i.e., NO_2, CN), an intense absorption is present below $\lambda = 265$ nm, which features a weak shoulder, near $\lambda = 340$ nm for **1-NO$_2$**, whereas a distinct weaker peak is detected near $\lambda = 281$ nm for the cyano derivative **1-CN** (see the Supporting Information). Otherwise, when the *para*-substituents become strongly electron-releasing (X = NH_2, NMe_2), an intense absorption is detected in the range $\lambda = 250$–270 nm with a shoulder at a higher wavelength (Figure 3). This absorption is bathochromically and hyperchromically shifted with the increasing electron-releasing power of the *para*-substituent. Based on these substituent-induced shifts, the most intense absorption likely corresponds to a symmetry allowed π*←π charge-transfer (CT) transition, the polarization of which depends on the nature (i.e., donor or strong acceptor) of the X substituent.[12d] Thus, when the substituent is neutral-to-strongly electron releasing, the CT takes place from the X substituent toward the electron-deficient isocyanurate core. The weak shoulder, always apparent on the low-energy side, certainly corresponds to a weakly allowed transition. The latter is likely a carbonyl π*←n transition according to DFT (see

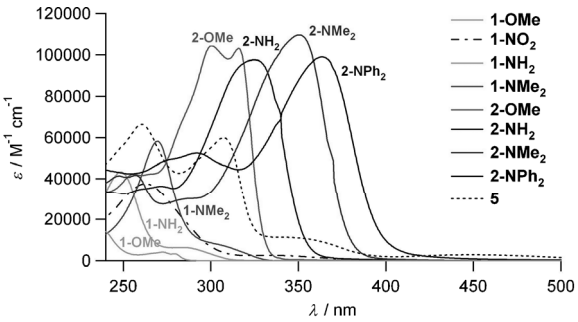

Figure 3. UV/Vis spectra for selected derivatives **1-X**, **2-X**, and **5** in dichloromethane ($T = 20$ °C).

Table 2. Absorption and emission properties of selected cyclotrimers in dichloromethane at 25 °C.

Cmpd	λ_{abs} [nm]	ε_{max} ($\times 10^{-3}$) [$M^{-1}cm^{-1}$]	λ_{em} [nm]	ϕ[a]	Stokes shift [cm^{-1}][b]	DFT[c] λ_{max} [nm] (f) vacuum	DFT[c] λ_{max} [nm] (f) CH_2Cl_2	DFT[c] λ_{em} [nm] (f) CH_2Cl_2
1- OMe	272 (sh)	4.1	297	0.006	3100	243 (0.0006)	247 (0.0002)	n.c.[d]
	234	25.0		–	–	220 (0.13)	220 (0.19)	
1-NH$_2$	286 (sh)	6.5	320	0.010	3700	256 (0.0004)	261 (0.0006)	n.c.[d]
	248	54.2		–	–	224 (0.20)	229 (0.24)	
1-NMe$_2$	316 (sh)	8.5	350	0.011	3100	269 (0.0003)	275 (0.0013)	n.c.[d]
	270	58.2		–	–	239 (0.22)	250 (0.58)	
2-OMe	316	106.4	348	0.025	4600	324 (1.87)	333 (2.03)	394 (1.87)
	300	104.4			–	–	–	
	264	44.4			–	245 (0.05)	247 (0.12)	
	254	44.4						
2-NH$_2$	326	97.6	396	0.056	5400	335 (1.70)	336 (1.74)	412 (0.25)
	272	44.0			–	253 (0.04)	254 (0.13)	
2-NMe$_2$	352	109.6	418	0.200	4500	349 (1.88)	375 (2.00)	423 (1.91)
	288	34.1			–	264 (0.16)	266 (0.49)	
2-NPh$_2$	364	99.0	437	0.730	4600	388 (1.90)	404 (1.95)	472 (1.16)
	294	56.4			–	296 (0.75)	298 (0.80)	
3-H	278 (sh)	5.5	301	0.025	2800	256 (0.07)	–[f]	
	251	74.3		–	–	249 (0.47)	253 (0.49)	311 (0.98)
5	436	2.7	NF[e]	–	–	n.c.[d]	n.c.[d]	n.c.[d]
	342 (sh)	11.4						
	307	57.0						
	260	66.4						

[a] Fluorescence quantum yield in CH_2Cl_2 when excited at λ_{abs} (quinine bisulfate in H_2SO_4 (0.5 M) was used as a standard). [b] Stokes shift = $(1/\lambda_{abs} - 1/\lambda_{em})$. [c] f = oscillator strength. [d] n.c. = not computed. [e] NF = no fluorescence detected. [f] Not found by DFT.

the Computational section). When the unsaturated arms are extended, that is, when progressing from **1-X** to **2-X** for a given electron-releasing substituent, further bathochromic and hyperchromic shifts are observed for this transition, and the intense band of the **2-X** cyclotrimer now overlaps with the low-energy absorption that appears as a shoulder in the **1-X** homologues.[29] In spite of its shift, the absorption at the longest wavelength remains in the UV range in line with the colorless appearance of these compounds in solution, except for **2-NPh$_2$**, which is faint yellow.

In contrast to the organic derivatives, the tris-ferrocenyl compound **5** has an intense brown–orange color in solution. This color is attributable to a weak absorption observed at $\lambda = 436$ nm for this complex, which possibly corresponds to ferrocenyl-based d←d transitions.[30] On the basis of previous reports, the absorption at $\lambda = 342$ nm could typically correspond to a $(\pi^*)_{CT} \leftarrow d_{Fe}$ metal-to-ligand charge-transfer (MLCT) transition, whereas the intense absorptions near $\lambda = 310$ nm and its shoulder may be attributed to MLCT processes. Finally, in connection with the substituent effect previously discussed for the **1-X** cyclotrimers, it is tempting to assign the absorption detected at $\lambda = 260$ nm to a $\pi^* \leftarrow \pi$ transition similar to that observed for **3-H** at $\lambda = 251$ nm. Indeed, based on well-known electronic substituent effects,[31] the ferrocenyl group is more electron releasing than a hydrogen atom and could lead to a bathochromic shift of this band.

Luminescence studies: The cyclotrimer families **1-X** and **2-X** also proved to be luminescent, their luminescence being strongly dependent on the size and on the nature of X (see Figure 4, Table 2, and the Supporting Information). Thus, compounds **1-X** exhibit low fluorescence quantum yields (< 1%), in agreement with the lowest-lying $\pi^* \leftarrow$n transition. Increasing the electron-releasing character of the peripheral X substituents leads to a bathochromic shift of the intense emission band and a small increase in the fluorescence quantum yield from 0.4–0.5% for the Me and H groups to 1.1–1.2% for the amino groups. The latter parallels the increase in the molar extinction coefficients observed for the lowest-lying intense transition (i.e., from 800–1000 $M^{-1}cm^{-1}$ for H and Me groups to 6000–7000 $M^{-1}cm^{-1}$ for the amino groups; Table 2). This transition, ascribable to the $\pi^* \leftarrow$n transition, appears as a shoulder on the low-energy side of the main absorption band for the **1-X** cyclotrimers (see Figure 3 and the Supporting Information). For a given X substituent, the extended compounds **2-X** are always more emissive than the smaller compounds **1-X**; furthermore, among the **2-X** derivatives, those with the most electron-releasing X substituents are more luminescent. They also present the most marked redshifts of the $\pi^* \leftarrow \pi$ transition, which becomes the lowest-energy transition in these derivatives (X=NR$_2$). An increase in the length of the π-electron system that connects the isocyanurate core to the peripheral X substituents also induces a bathochromic shift of the emission band and a marked increase in the quantum yields (up to 73% for **2-NPh$_2$**). In contrast to these purely organic derivatives, metallated complex **5** was not luminescent at all. The luminescence of this particular compound is possibly quenched by electron transfer from the electroactive ferrocenyl groups.[32]

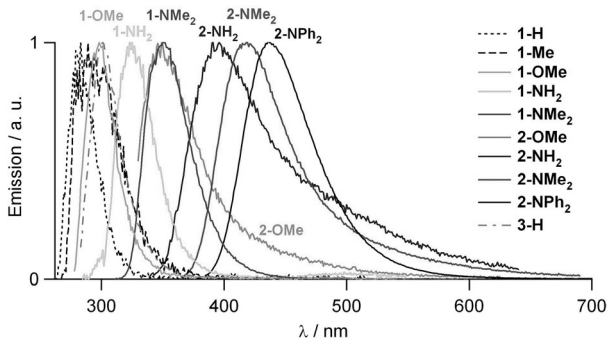

Figure 4. Normalized emission spectra for selected derivatives **1-X**, **2-X**, and **3-H** in dichloromethane ($T = 20$ °C).

Solvatochromism: In line with the absence of a permanent dipole moment in these molecules in the ground state, quasi-negligible solvatochromic behavior could be stated for the absorption of most of the **1-X** derivatives (see Figure 5 and the Supporting Information).[33] A very slight solvatochromism is nevertheless observed in the absorption of compounds **2-X** featuring amino substituents. Thus, an overall negative solvatochromism takes place for **2-NPh$_2$** and **2-NMe$_2$** ($\Delta\nu_{max} = <540$ and <580 cm^{-1}, respectively), whereas a larger and overall positive solvatochromism is observed for **2-NH$_2$** ($\Delta\nu_{max} = <1090$ cm^{-1}). These contrasting behaviors cannot be related to the purely dipolar effect of the solvent and suggest that solvent specific effects are operative. During the emission process, however, the extended cyclotrimers **2-X** exhibit a much larger solvatochromism, as evidenced below for **2-NPh$_2$** (Figure 5). An increase in the solvent polarity induces a marked bathochromic shift of their emission band. Their solvatochromic behavior follows the Lippert–Mataga relationship[35] [see Eq. (1a) and the Supporting Information] with a linear dependency of the Stokes shift on the polarity–polarizability parameter Δf [Eq. (1b)]:

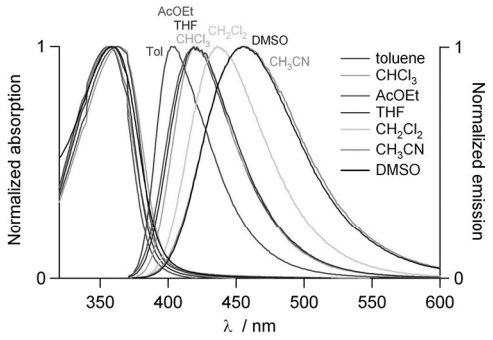

Figure 5. Solvatochromic absorption and emission behavior of **2-NPh$_2$** in various solvents ($T = 25$ °C).

$$\tilde{\nu}_{abs} - \tilde{\nu}_{em} = 2\Delta\mu^2\Delta f/(hca^3) + \text{const} \quad (1a)$$

where, ν_{abs} and ν_{em} are the wavenumbers of the absorption and fluorescence maxima, respectively; h is the Planck constant; c is the light velocity; a is the radius of the solute spherical cavity; $\Delta\mu$ is the change of dipole moment between the ground state and the emitting excited state; and Δf is defined as:

$$\Delta f = (\varepsilon-1)/(2\varepsilon+1) - (n^2-1)/(2n^2+1) \quad (1b)$$

where ε is the dielectric constant and n is the refractive index of the solvent. This behavior, already reported earlier for other octupolar derivatives built from a triphenylamine core,[36] is indicative of a highly polar emissive excited state that results from excitation localization on a dipolar branch after excitation, prior to emission.[37]

Two-photon absorption (TPA) studies: By using the luminescence of these compounds, we tried to determine their TPA cross sections in the near-IR (NIR) range (λ=700–1000 nm) through investigation of their two-photon excited fluorescence (TPEF). The excitation was performed with femtosecond pulses from a Ti:sapphire laser (Figure 6 and Table 3). However, due to instrumental limitations, no TPEF could be detected for many of these compounds in the available spectral range of the laser because the **1-X** cyclotrimers have their OPA below λ=350 nm (which is also the case for **2-OMe**). In contrast, the amino derivatives **2-X** exhibit significant TPEF in the NIR range, and their fluorescence quantum yield is large enough for accurate determination of their TPA cross sections. Only the red edge of the TPA band could be obtained for cyclotrimer **2-NH$_2$**, whereas the maximum of the TPA band was observed for **2-NMe$_2$** and **2-NPH$_2$** and is located at λ=720 and 740 nm, respectively, with high maximum TPA cross sections (up to 410 GM). Extension of the π-conjugated connectors and an increase in the strength of the donor terminal groups was therefore a fruitful way not only to enhance the photoluminescence properties, but also to obtain good two-photon absorbers at the beginning of the NIR range. The comparison of the TPA band of **2-NMe$_2$** and **2-NPh$_2$** with their rescaled one-photon band shows that the TPA maximum is situated close to twice that of the OPA maximum. This comparison also suggests that the excited states at the origin of the TPA absorption in the NIR are also active in OPA and correspond to the most intense one-photon transitions detected at the lowest energy in the UV range (see the Supporting Information).

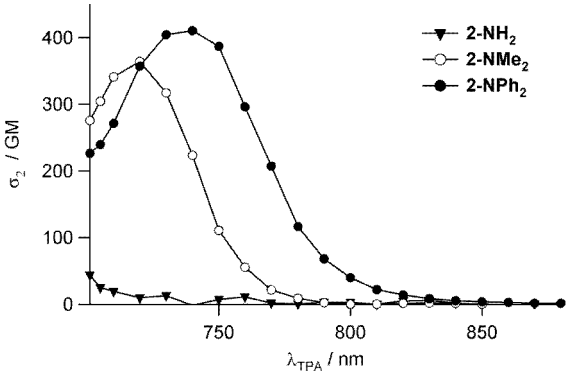

Figure 6. TPA spectra of **2-X** (X=NH$_2$, NMe$_2$, NPh$_2$) in dichloromethane (T=25°C) in the NIR range.

Table 3. TPA properties of selected cyclotrimers in dichloromethane at 25°C.

Cmpd	λ_{OPA}[a] [nm]	λ_{TPA}[b] [nm]	σ_2[c] [GM]	σ_2/MW[d] [GM g^{-1}]	$\phi\times\sigma_2$[e] [GM]
2-NH$_2$	326	≤700	≥45	≥0.06	>2.5
2-NMe$_2$	352	720	360	0.458	72
2-NPh$_2$	364	740	410	0.354	300

[a] Maximum of the OPA. [b] Maximum of the TPA. [c] TPA cross section at the maximum. [d] Figure of merit relevant for applications in optical limiting or nanofabrication.[38] [e] Two-photon brightness relevant figure of merit for imaging applications. ϕ=luminescence quantum yield, MW=molecular weight.

DFT calculations: Compounds **1-OMe**, **1-NH$_2$**, **1-NMe$_2$**, **3-H**, **2-OMe**, **2-NH$_2$**, **2-NMe$_2$**, **2-NPh$_2$**, and **3-H** were employed for the DFT calculations (see the Computational Details). The solid-state geometry found for **3-H** (Table 1) was used to generate the various structures before optimization, which was then performed without symmetry constraints for all the derivatives. For calculation purposes (see later), the structure of the isocyanuric acid trimer **6** (Scheme 1; R=H for **A**) was also derived from **3-H** and optimized.

For the model compound **3-H**, the calculated geometric parameters compare well with the experimental data (see Table 1 and the Supporting Information). The three peripheral 4-phenylethynyl substituents adopt a tilted conformation relative to the isocyanurate mean plane in the optimized geometry, thus resulting in a pseudo-D_3 symmetry, very similar to the D_3 geometry observed in the solid-state structure of this compound (Figure 7). The experimental C8-C7-N3-C4 dihedral angle is −83.41°, and the calculated angles are −67.69 and −89.30° in the gas phase and dichloromethane, respectively. Notably, the computed parameters in a dielectric continuum that correspond to dichloro-

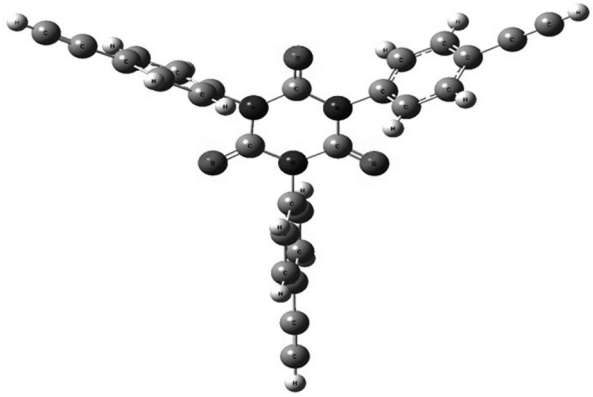

Figure 7. Optimized geometry of **3-H**.

methane are closer to the experimental data than those obtained in the gas phase. Indeed, the mean deviations in the gas phase and solution are 0.008 and 0.007 Å for the bond lengths, 1.40 and 0.92° for the bond angles, and 3.08 and 1.85° for the torsion angles, respectively.

With the exception of the methoxy derivatives **1-OMe** and **2-OMe**, which featured differently oriented methoxy groups, pseudo-D_3 geometries were also found for all the other compounds after optimization without symmetry constraints. In the case of the extended compounds **2-OMe**, **2-NH$_2$**, **2-NMe$_2$**, and **2-NPh$_2$**, the two phenyl rings remain coplanar within each arm and each arm adopts a similarly tilted conformation relative to the central isocyanurate core. As expected from the overall symmetry of these molecules, the dipole moment in their ground state is essentially zero, except for the compounds that bear methoxy groups. Indeed, the latter rotate during the optimization procedure and give rise to slight dipole moments in the range 1.5–2.0 D with large out-of-plane contributions (Table 4). A comparison between the computed vibrational modes and experimental values also proved satisfactory because they confirmed the attribution proposed for the isocyanurate-based ν_{CO} modes (see the Supporting Information).

Table 4. Calculated dipole moments and HOMO–LUMO gaps for **1-OMe**, **1-NH$_2$**, **1-NMe$_2$**, **2-OMe**, **2-NH$_2$**, **2-NMe$_2$**, **2-NPh$_2$**, and **3-H**.

Cmpd	μ [D]		HOMO–LUMO gap [eV]	
	Vacuum	CH_2Cl_2	vacuum	CH_2Cl_2
1-OMe	1.33	1.65	5.74	5.70
1-NH$_2$	0.31	0.38	5.58	5.47
1-NMe$_2$	0.20	0.03	5.21	4.92
2-OMe	1.49	1.70	4.12	4.09
2-NH$_2$	0.56	0.07	3.98	3.81
2-NMe$_2$	0.41	0.63	3.82	3.61
2-NPh$_2$	0.03	0.08	3.56	3.46
3-H	0.00	0.01	5.20	5.26

Although the models studied were optimized without symmetry constraints, and therefore no longer belonged to the D_{3h} symmetry group to which the idealized starting geometry belonged, the local (C_3) pseudosymmetry around the isocyanurate core allows recognition of MOs that would belong to the A or E representations with the C_3 symmetry. Thus, as with **3-H**, the HOMOs of **1-OMe, 1-NH$_2$**, and **1-NMe$_2$** belong to the symmetric (A) representation with π-type MOs that are essentially located on the periphery of each cyclotrimer and present a sizeable weight on the donor substituent (ca. 23, 30, and 44% for **1-OMe**, **1-NH$_2$**, and **1-NMe$_2$**, respectively; Figure 8). HOMO-1 and HOMO-2 are nearly degenerate in energy and can be identified with two sister MOs that would belong to an E irreductible representation under an ideal C_3 or D_3 symmetry (Figure 9a). The LUMO and LUMO+1 of these compounds also seem to constitute a degenerate pair of E-type MOs that are essentially π based, but also heavily weighted on the carbonyl antibonding $(\pi_{CO})^*$ and somewhat on the π* MOs of the first phenyl ring linked to the isocyanurate core. In contrast,

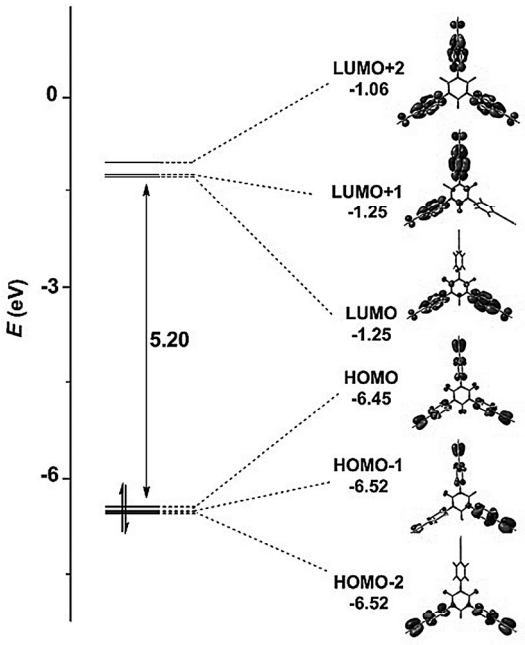

Figure 8. Frontier molecular orbitals of **3-H** (optimized geometry).

LUMO+2 belongs to a totally symmetric representation (A) and essentially results from a combination of π* MOs of the first phenyl rings connected to the isocyanurate core. For the longer compounds **2-OMe**, **2-NMe$_2$**, and **2-NPh$_2$**, the HOMO is rather similar and now includes the alkynyl bond (Figure 9b). As a result, the weight of the terminal donor atom slightly decreases relative to the shorter compounds (9, 18, and 26% for **2-OMe**, **2-NH$_2$**, and **2-NMe$_2$**, respectively). More in contrast to the **1-X** compounds, the LUMO to LUMO+2 are now essentially located on the π manifold of the peripheral arms, and do not include any sizeable $(\pi_{CO})^*$ character.

Rather large HOMO–LUMO gaps separate the empty antibonding MOs from the HOMOs (5.74–5.20 eV) in the shortest cyclotrimers **1-X** and **3-H**. This gap progressively decreases upon elongation of the π manifold on the peripheral arms, that is, when progressing from **1-X** to **2-X**. The gap also decreases among each series, especially when more and more electron-releasing substituents are present on the periphery (Table 4), thereby mirroring the variation in energy of the lowest-lying intense absorptions of these compounds (Table 2).

The lower-lying electronic transitions were then derived by time-dependent DFT (TD-DFT) calculations under vacuum and in dichloromethane (see the Supporting Information). Consideration of a dielectric continuum around the molecules results in a change in the nature of the low-energy transitions for the **1-X** and **3-H** systems and in a slight improvement in the overall oscillator strength, which is inline with non-negligible solvation effects. The first intense ($f>0.13$) transition corresponds to a symmetry-allowed π*←π transition (E←A). The main character of this transition is the transfer of electron density between essen-

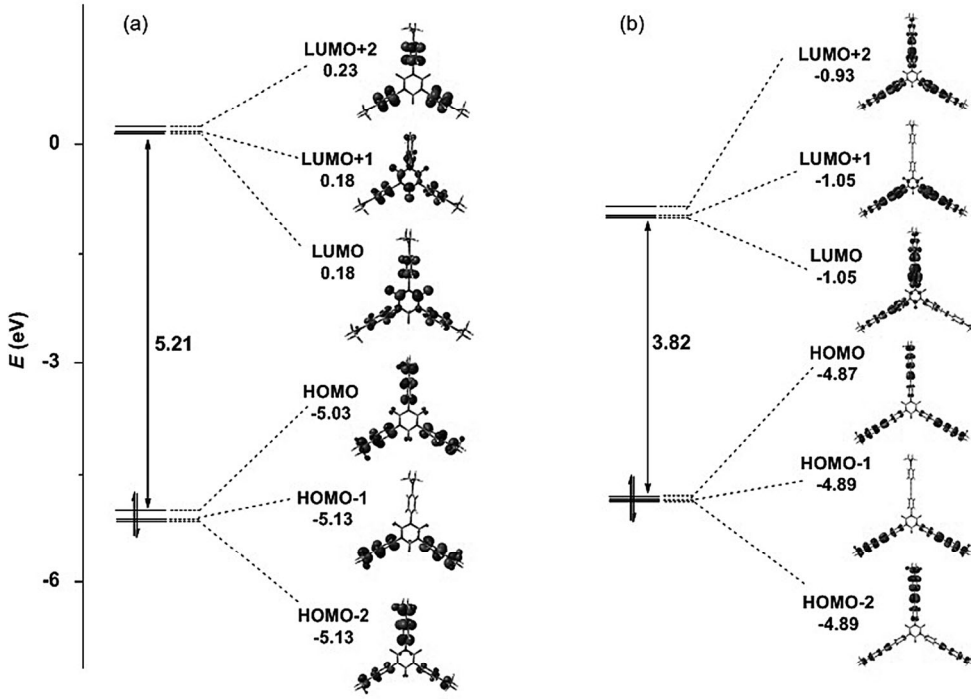

Figure 9. Energy diagram of the molecular frontier orbitals of the a) **1-NMe$_2$** and b) **2-NMe$_2$** systems in their optimized geometry.

tially phenyl-based π manifolds on each arm from the periphery toward the center of the compound, with some $(\pi_{CO})^*$ character present in the vacant MOs, but only in the shortest compounds (i.e., **1-X** and **3-H**). For **2-X** compounds, an increase in the overall $\pi^*\leftarrow\pi$ character of this transition within each arm is stated relative to the shorter homologues **1-X** (X=OMe, NH_2, NMe_2). According to calculations, although this transition involves the very frontier MOs in the longer compounds (**2-X**), this transition does not correspond to the HOMO–LUMO transition for the shorter compounds (**1-X**) and also does not correspond to the experimentally detected shoulder that appears on the low-energy edge of their lowest-lying intense absorption. The latter might be attributed to weakly allowed transitions of $(\pi^*)_{CO}\leftarrow n_O$ character, more specific to the isocyanurate core. Their exact nature was more easily unraveled by TD-DFT computations performed on model compound **6**, which lacks peripheral phenyl groups (Figure 10) and is a model that plainly demonstrates these LUMO←HOMO and LUMO+1←HOMO transitions that are partly forbidden by symmetry. The wavelength of these transitions was computed to be at $\lambda=214$ nm for **6**. For the longer derivatives **2-X**, a second weaker E←A transition energy (LUMO←HOMO-3 and LUMO+1←HOMO-3) should in principle take place at higher energy, as experimentally observed. Thus, the effects of the arms extension and the substituents on these transitions are qualitatively well reproduced. Overall, the match with our experimental observations is good (Table 2) and, qualitatively, the effect of the arms extension and electronic substituent effects on these transitions is well reproduced.

Also, emission energies from the relaxed excited-state geometry were computed for **2-X** and **3-H** in dichloromethane (see Table 2 and the Supporting Information). The computed wavelengths and oscillator strengths correspond to an emission from the relaxed first singlet excited state, and the optimized geometry was computed by using TD-DFT calculations. According to these calculations, a strongly allowed emission should be observed above $\lambda=350$ nm for **2-OMe**, **2-NMe$_2$**, and **2-NPh$_2$**. All these emissions originate from LUMO→HOMO transitions. Again, in terms of energies, the TD-DFT results correlate nicely with the experimental data (Table 2), albeit slightly overestimated for each compound. Also, the oscillator strengths computed for these compounds (especially **2-OMe** and **2-NPh$_2$**) do not always reflect the quantum yields measured experimentally in dichloromethane. These discrepancies might originate from the fact that the true emitting state was not always found by using our computational procedure. Alternatively, by considering the energetic proximity between the $(\pi^*)_{CO}\leftarrow n_O$ and LUMO←HOMO states in these cyclotrimers, if the former is

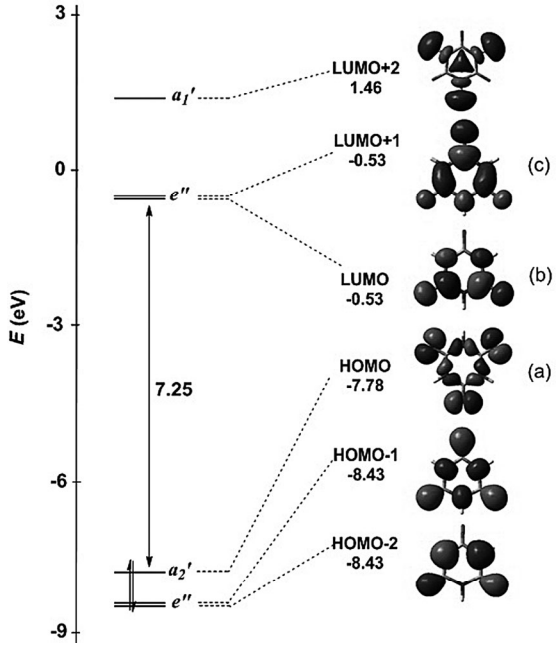

Figure 10. Frontier MOs of **6** (D_{3h} symmetry): a) HOMO, b) LUMO, and c) LUMO+1.

slightly more stabilized in the real compounds than in the computations, lower radiative rates will result. Then, in connection with the strong solvatochromism observed in the emission (see Figure 5 and the Supporting Information), DFT computations reveal the buildup of polarity oriented along one of the arms of the cyclotrimer that accompanies the vibronic relaxation in the gas phase of the first excited singlet.[11a,37b] Due to this process, the dipole moments increase significantly relative to the ground state from 1.49 to 7.28 D for **2-OMe** and from 0.41 D to 11.78 D for **2-NMe$_2$**.

Finally, the hyperpolarizabilities were computed by finite differences with B3LYP/6-31G* calculations (Table 5) and by using AM1 calculations (see the Supporting Information).[39] The solvent polarity seems to have only a moderate influence on the β values computed, except for **2-OMe** and **2-NPh$_2$**, for which significantly larger hyperpolarizabilities were found in dichloromethane.

Table 5. Molecular hyperpolarizabilities and related experimental (HRS at $\lambda = 1907$ or 1064 nm)[14] and theoretical DFT data derived for selected cyclotrimers in dichloromethane.

Cmpd	λ_{max}[a] [nm]	β_{HRS}[b]	$\beta_{HRS}(0)$[c]	$\|\|\beta\|\|$ [10^{-30} esu]	$\|\|\beta_0\|\|$	$\beta_{DFT}(0)$[d] vacuum	$\beta_{DFT}(0)$[d] CH_2Cl_2	$\|\|\beta_0\|\|/MW$[e] [10^{-32} esu g^{-1}]
1-OMe	228	19[f]	15[f]	62	48	0.2	0.3	0.107 (0.001)
1-NH$_2$	248	–[g]	–[g]	–	–	0.6	0.8	–[g] (0.002)
1-NMe$_2$	270	55	50	178	161	1.5	2.2	0.330 (0.005)
2-OMe	316	32[f]	19[f]	104	61	13.9	24.9	0.082 (0.033)
2-NH$_2$	326	–[g]	–[g]	–	–	20.2	26.8	–[g] (0.038)
2-NMe$_2$	352	66	55	214	178	32.5	32.7	0.227 (0.042)
2-NPh$_2$	362	78	64	253	209	50.4	98.9	0.180 (0.085)

[a] In solution with CH_2Cl_2. [b] The precision of the measurements is about $\pm 15\%$; ethyl violet ($\beta = 170 \times 10^{-30}$ esu) was used as the reference in CH_2Cl_2; correlation between SI units: $\beta(SI) = 4.172 \times 10^{-10} \beta$ (esu); the reported β values are given in the β^X convention as defined by Willets et al.[40] [c] Calculated by using Equation (2a). [d] Values calculated for vacuum and solution. [e] Values deduced from theoretical values are given in parenthesis. [f] The measurement was performed in $CHCl_3$ at $\lambda = 1064$ nm; the solvent ($\beta = 0.19 \times 10^{-30}$ esu) was used as a reference at this wavelength. [g] Not determined due to low solubility.

Discussion

Linear optical properties: Linear absorption studies reveal that cyclotrimers such as **1-X** or **2-X** present an intense allowed transition in the UV range, whereas a second transition at higher energy is detected for the extended derivatives. The most intense transitions in the UV range for these compounds are reproduced fairly well by nonsymmetry-restricted TD-DFT calculations (Table 2), thus revealing a correspondence to a symmetrical charge shift from the periphery toward the center of the arms, with a strong $\pi^* \leftarrow \pi$ character. A simple symmetry-based analysis (Frenkel exciton model) of compounds that possess a trifold symmetry axis predicts that any set of arm-localized CT transitions combine to give two new symmetry-adapted transitions in such octupolar systems.[11a,d,37b,41] One transition, nondegenerate and one-photon forbidden, belongs to an A-type irreducible representation, and the other transition, doubly degenerate and one-photon allowed (as well as two-photon allowed), belongs to a E-type representation. In the absence of electronic interactions between branches, these two transitions should take place at the same energy, but in case of a sizeable electronic coupling, the E$\leftarrow$A-type transition should be lower in energy. Accordingly, TD-DFT computations confirm that the strong transition detected each time for **1-X** or **3-H** cyclotrimers corresponds to a E$\leftarrow$A-type transition, whereas the shoulder detected at lower energy is assigned to forbidden $(\pi^*)_{CO} \leftarrow n_O$ transitions. The intense (allowed) E$\leftarrow$A transition is controlled by the nature of the donor groups and by the length of the conjugated arms. Thus, increasing the electron-releasing power of the X substituent raises the HOMO energy, thereby decreasing the HOMO/LUMO gap. Alternatively, upon extension of the arms, the $(\pi^*)_{CO}$ character of the LUMO decreases concomitantly with an increase in ethynyl character for both the HOMO and LUMO. These electronic effects contribute to a decrease in the HOMO–LUMO gap and, while shifting the corresponding $\pi^* \leftarrow \pi$ transition to lower energies, strengthen its arm-centered character. However, this transition remains in the UV range for all the organic cyclotrimers tested so far, even the extended ones that feature amino substituents. As a result, **1-X** and **2-X** present a good transparency range in the visible range, with only a slight yellowish color being observed for **2-NPh$_2$** in solution. In line with their quasi-nonpolar ground state, a very weak solvatochromism is observed in absorption.

Luminescence studies reveal that these compounds are also emissive, especially the longer **2-X** compounds bearing strong electron-releasing substituents. On the basis of the TD-DFT computations, the allowed (E$\leftarrow$A) transition should populate an excited state that is potentially strongly emissive and that presents a strong $\pi^* \leftarrow \pi$ CT character. The low fluorescence quantum yield observed for the shorter compounds is attributed to the existence of a weakly allowed $(\pi^*)_{CO} \leftarrow n_O$ transition, observed as a shoulder on the lower-energy side of the intense E$\leftarrow$A absorption band. Indeed, mirror images between the absorption and emission (see the Supporting Information) clearly reveal that the strongly absorbing state is not the emitting state for the **1-X** derivatives. This state of lower energy in **1-X** and **3-H** traps the initially generated $\pi^* \leftarrow \pi$ CT state (through fast internal conversion) and mostly decays in a nonradiative way to the ground state due to the low radiative rate of the lower emissive state according to the Strickler–Berg equation.[42] However, extension of the conjugation path within each arm and peripheral functionalization with donor groups bathochromically shifts the $\pi^* \leftarrow \pi$ CT state, whereas the $(\pi^*)_{CO} \leftarrow n_O$ transition remains unaffected. As a result, the strongly allowed (E$\leftarrow$A) transition becomes the lowest-energy transition, thus leading to strong emission for compounds **2-X** bearing strongly electron-releasing substituents. In agreement with the absence of a shoulder on the low-energy side in the absorption spec-

tra of these compounds, the radiative decay dominates the de-excitation pathways of the excited state. For the latter compounds, the marked positive solvatochromism stated in the emission gives rise to large slopes in the corresponding Lippert–Mataga plots. This behavior is indicative of a highly polar emissive excited-state that results from the localization of the excitation on one of the dipolar arms, as previously observed for other types of octupolar systems.[36,37] DFT calculations on the excited states agree with such an interpretation.

Nonlinear optical properties: The hyperpolarizabilities of the cyclotrimers **1-X** and **2-X** featuring electron-releasing groups at their periphery have been previously determined by the hyper Raleigh scattering (HRS) method in solution (Table 5), except for **1-NH$_2$** and **2-NH$_2$** which turned out to be not soluble enough.[14] The corresponding static hyperpolarizabilities, denoted as $\beta_{HRS}(0)$ hereafter, were determined by using the simple three-level model [Eqs. (2a) and (2b)].[10c,43] With an incident beam at 1907 nm (or 1064 nm), the difference between dynamic (β) and static hyperpolarizabilites (β_0) remains small for most of these compounds. The corresponding orientationally averaged hyperpolarizabilities ($\langle\beta^2\rangle$) were evaluated along with the modulus of the hyperpolarizability tensor ($||\beta|| = [\Sigma_{ijk}\beta_{ijk}^2]^{1/2}$), considering an idealized D_{3h} or D_3 symmetry for these NLO-phores and assuming that $||\beta||$ was essentially dominated by the in-plane longitudinal components ($||\beta|| = 2|\beta_{zzz}|$) [Eq. (3)].[10c,43]

$$\beta = \beta_0 \, [E_{01}^2/(E_{01}^2 - 4\hbar^2\omega^2)(E_{01}^2 - \hbar^2\omega^2)] \quad (2a)$$

$$\beta_0 = 3/2[|\mu_{01}|^2 \, \mu_{1-1}/E_{01}^2] \quad (2b)$$

$$|\beta_{zzz}| = (21/8)^{1/2}\beta_{HRS}(0) \quad (3)$$

An increase in the molecular hyperpolarizabilities was stated when increasing the donating power of the X substituent or when proceeding from **1-X** to **2-X** for a given X substituent. The theoretical values presently calculated by DFT reproduce this trend, but underestimate the values of the hyperpolarizabilities found experimentally (Table 5). It is important to point out here that our DFT calculations do not take into account any vibrational contribution[44] or specific solvation effects.[45] Similar differences between the experimental and theoretical values have precedence.[39,46] The mismatch with DFT values is most pronounced for the shorter compounds (**1-X**), but diminishes for the longer cyclotrimers (**2-X**). The AM1 calculations performed for these compounds also give overall lower values than the experimental values, but the molecular hyperpolarizabilities of the **1-X** and **2-X** compounds lie much closer (see the Supporting Information). Actually, the main discrepancy between the experiment and calculations resides in the inverse order found for the molecular hyperpolarizabilities of **1-NMe$_2$** and **2-OMe**.

The classic figures of merit ($||\beta_0||$/MW; MW = molecular weight) were also calculated for these compounds (Table 5). These data allow for comparison between different symmetries and sizes through MW normalization. On the basis of the experimental values, these figures of merit suggest that functionalizing the shorter **1-X** derivatives by strong donors (such as in **1-NMe$_2$**) constitute a better strategy to improve the NLO response of these compounds than synthesizing cyclotrimers with extended arms such as **2-X**. As previously discussed,[14] the hyperpolarizabilites determined for **1-X** (X = OMe, NMe$_2$) and **2-X** (X = OMe, NMe$_2$, NPh$_2$) are far from negligible when reported relative to the size of the molecules and stand comparison with the β_0 values reported for related octupoles (Scheme 7).[13] Without surprise, these derivatives present a much better hyperpolarizability than that previously determined for **11**, which features electron-

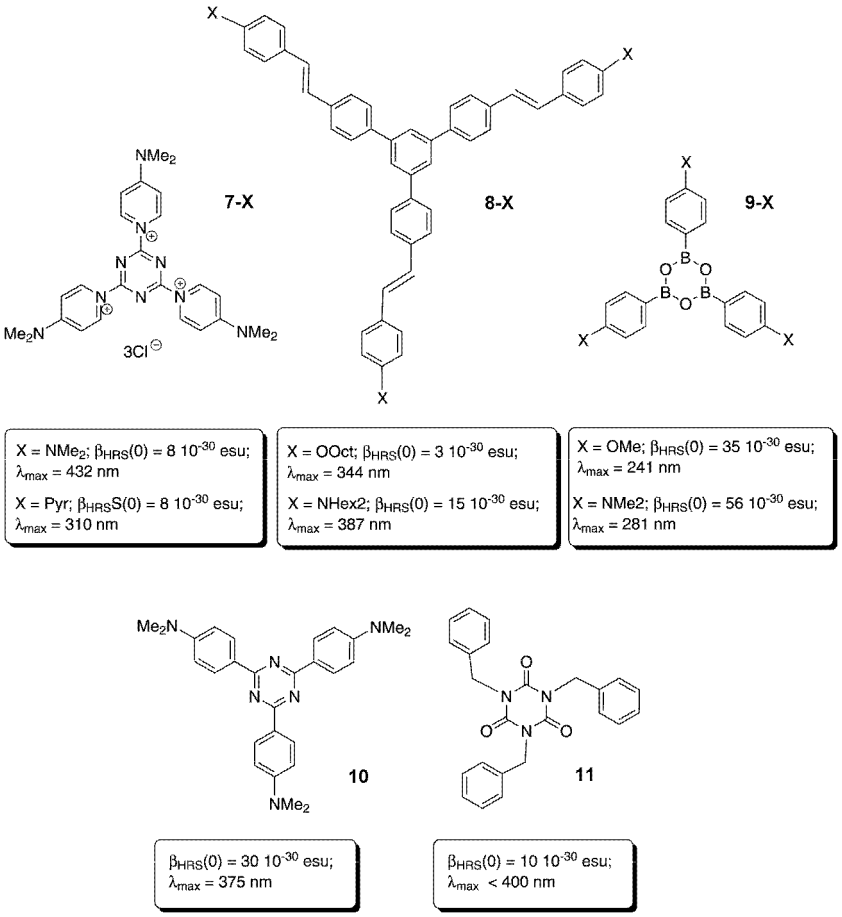

Scheme 7. Selected octupoles related to the cyclotrimers **1-X** and **2-X**.

poorer arms and for which no conjugation was effective between the peripheral arms and the central core.[9] Actually, the **1-X** and **2-X** derivatives presently studied possess an activity/transparency tradeoff comparable to that of the boroxines **9-X** previously studied by some of us.[47]

Considering a classic VB model of a simple D_3 compound with three CT states, we know that TPA is symmetry allowed from the ground state to both the E- and A-type (lower and higher in energy, respectively) states.[11a,37b,48] Accordingly, the TPA peak matches well with half of the energy of the intense peak in the UV range also attributed to this transition. When compared to the values determined for other propeller-shaped octupolar derivatives of the same size and bearing electron-releasing substituents at the periphery, the TPA cross sections found for **2-NMe$_2$** and **2-NPh$_2$** are rather similar to those values reported for triaryl benzenes such as **8-NHex$_2$** ($\sigma_2 = 407$ GM),[49] but are clearly larger than those values reported for triarylamino derivatives such as **12** ($\sigma_2 = 30$ GM;[36a] Scheme 8). Notably, the figures of merit classically considered for application in optical limiting or nanofabrication, such as σ_2/MW (Table 3), which were obtained for **2-NMe$_2$** or **2-NPh$_2$**, are comparable or better than those values obtained for **7-NHex$_2$** or **12**.[38c] This outcome is however no longer the case when octupoles that can adopt a fully conjugated planar conformation, such as **13** ($\sigma_2 = 2405$ GM), are considered.[50] Given that the **2-X** molecules were presently not optimized for TPA, these results are strongly encouraging to investigate the TPA properties of new analogues of these cyclotrimers further. In particular, it would be interesting to investigate related derivatives in which the triple bond would be replaced by a double bond, which should result in combined redshift and TPA enhancement.[51] As a result, the TPA band that corresponds to the intense band of the two-photon allowed A←A transition[37b] would be shifted in the NIR range, thus leading to a major enhancement.[36b]

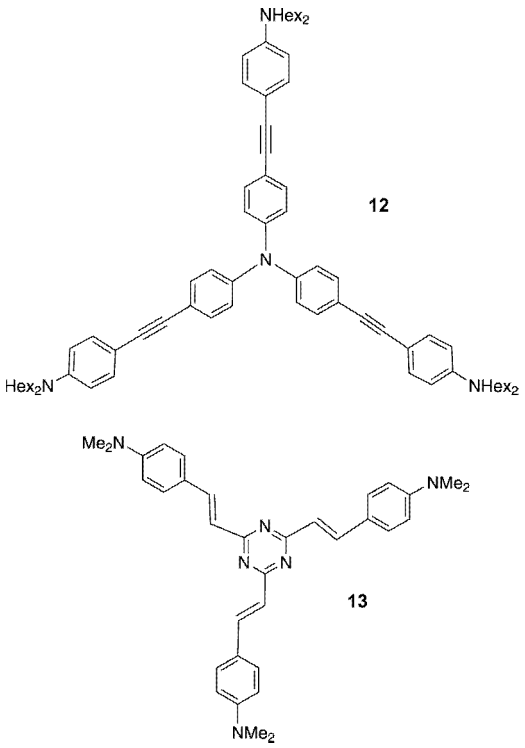

Scheme 8. Selected two-photons absorbers related to the cyclotrimers **2-X**.

Conclusion

For the first time, an extensive study of the linear and nonlinear optical properties of a series of isocyanurates functionalized by donor arms at the periphery has been conducted. Although some of the shorter derivatives among **1-X** or **5** were already known, the longer derivatives **2-X** and **3-X** reported herein are new molecules that have been fully characterized. These compounds, previously demonstrated by some of us to present a good activity/transparency tradeoff in terms of second-order NLO activity,[14] are readily accessible in a few steps from commercial isocyanates. We also showed that the longer derivatives **2-X**, when functionalized with strong donor groups (X = NH_2, NMe_2, or NPh_2), become strongly luminescent and exhibit fairly large TPA cross sections (with σ_2 values up to 410 GM). DFT calculations reveal their electronic structures and confirm the trends previously evidenced by HRS for their hyperpolarizabilities.[14] The origin of these hyperpolarizabilities can be traced to the existence a strong octupolar CT transition (of E←A symmetry) from the peripheral arms toward the isocyanurate core that takes place in the near-UV range. This latter transition becomes the lowest-lying transition for the **2-X** derivatives with extended arms. Although the HRS measurements did not demonstrate basically enlarged hyperpolarizabilities for the extended derivatives **2-X** over their **1-X** analogues, TPEF studies pointed out that **2-X** constitute the first members of a new class of promising biphotonic absorbers. Work is in progress to explore new derivatives of this kind and to exploit their remarkable optical properties in molecular-based devices.

Experimental Section

General procedures: All the manipulations were carried out in an inert atmosphere of argon with dried and freshly distilled solvents. Commercial reagents (isocyanates) were used as received. Apart from **1-H**, some **1-X** cyclotrimers have been previously reported (**1-NO$_2$**[15b,d,18] **1-Br**,[15b] **1-Me**,[15a,18b] **1-OMe**,[2e,15a,b] and **1-NMe$_2$**)[15b] (see the Supporting Information for more details).

Catalytic cyclotrimerization reaction—general procedure: In an oven-dried Schlenk tube, cesium fluoride (2 mol%) was added to the isocyanate precursor dissolved in nitrobenzene (5–10 mL). The reaction mixture was stirred overnight at room temperature to give, in some cases, a pale precipitate. A mixture of diethyl ether/hexane (1:1) was added and the crude solid formed was filtered on a fritted funnel, before being purified by flash chromatography on silica gel.

1,3,5-Tris(4-cyanophenyl)-1,3,5-triazinane-2,4,6-trione (1-CN): Following the general procedure with 4-cyanophenylisocyanate (1 g, 6.9 mmol), CsF (21 mg, 0.14 mmol), and ethyl acetate as the eluent for chromatography

(250 mg, 25%). ^{1}H NMR (200 MHz, $CDCl_3$, TMS): δ=7.86 (d, $^3J_{H,H}$= 8.6 Hz, 6H), 7.56 ppm (d, $^3J_{H,H}$=8.6 Hz, 6H); $^{13}C\{^1H\}$ NMR (400 MHz, $CDCl_3$, TMS): δ=147.0, 136.3, 133.1, 129.2, 117.2, 113.8 ppm; IR (KBr): $\tilde{\nu}$=2229 (C≡N, m), 1779 (C=O, vw), 1714 cm^{-1} (C=O, s); Raman: $\tilde{\nu}$= 2230 (C≡N, vs), 1777 cm^{-1} (C=O, m); UV/Vis (CH_2Cl_2): λ_{max} (ε)=281 nm (17600 $mol^{-1}dm^3cm^{-1}$); MS (EI): *m/z* calcd for $C_{24}H_{12}N_6O_3$: 432.0970 $[M]^+$; found: 432.0965; crystals of X-ray quality were grown by slow diffusion of pentane into a solution of **1-CN** in acetone.

1,3,5-Tris(4-bromophenyl)-1,3,5-triazinane-2,4,6-trione (1-Br): Following the general procedure with 4-bromophenylisocyanate (4 g, 20.2 mmol), CsF (61 mg, 0.4 mmol), and CH_2Cl_2 as the eluent for chromatography (3.50 g, 88%). ^{1}H NMR (200 MHz, CD_2Cl_2, TMS): δ=7.75 (d, $^3J_{H,H}$= 8.7 Hz, 6H), 7.35 ppm (d, $^3J_{H,H}$=8.7 Hz, 6H); $^{13}C\{^1H\}$ NMR (50 MHz, CD_2Cl_2, TMS): δ=148.5, 133.2, 133.1, 130.6, 124.0 ppm; IR (KBr): $\tilde{\nu}$= 1776 (C=O, vw), 1719 cm^{-1} (C=O, vs); Raman: $\tilde{\nu}$=1772 cm^{-1} (C=O, s); λ_{max} (ε)=<230 (≥40000), 264 nm (1520 $mol^{-1}dm^3cm^{-1}$); UV/Vis (CH_2Cl_2): λ_{max} (ε): 264 nm (1520 $mol^{-1}dm^3cm^{-1}$); HRMS (EI) *m/z* calcd for $C_{21}H_{12}N_3O_3Br_3$: 592.8408 $[M]^+$; found: 592.8397; elemental analysis calcd (%) for $C_{21}H_{12}N_3O_3Br_3$: C 42.46, H 2.04, N 7.07; found: C 42.24, H 2.07, N 6.97; crystals of X-ray quality were grown by slow evaporation of a solution of **1-Br** in CH_2Cl_2.

1,3,5-Tris(4-aminophenyl)-1,3,5-triazinane-2,4,6-trione (1-NH$_2$) via 1,3,5-tris(4-nitrophenyl)-1,3,5-triazinane-2,4,6-trione (1-NO$_2$): Following the general procedure with 4-nitrophenylisocyanate (1.3 g, 7.9 mmol) and CsF (24 mg, 0.16 mmol). After filtration, **1-NO$_2$** was obtained as a yellow solid (1.2 g). This crude material was used as follows: A solution of calcium chloride (1 g, excess) in water (20 mL) was added to **1-NO$_2$** and zinc dust (5 g, excess) in ethanol (100 mL). This mixture was heated to reflux for 3 h, cooled to room temperature, and filtered on a fritted funnel. The filtrate was extracted with CH_2Cl_2, washed with water, and dried over $MgSO_4$. After filtration and evaporation to dryness, the crude product was purified by column chromatography on silica gel with ethyl acetate to give a gray solid, which required oven drying (660 mg, 62%). ^{1}H NMR (200 MHz, CD_3SOCD_3, TMS): δ=7.00 (d, $^3J_{H,H}$=8.4 Hz, 6H), 6.58 (d, $^3J_{H,H}$=8.4 Hz, 6H), 5.28 ppm (s, 6H); $^{13}C\{^1H\}$ NMR (50 MHz, CD_3SOCD_3, TMS): δ=150.5, 149.6, 129.9, 123.9, 114.3 ppm; IR (KBr): $\tilde{\nu}$=3461, 3379 (NH, m), 1762 (C=O, vw), 1683 cm^{-1} (C=O, vs); Raman: $\tilde{\nu}$=3068 (NH, m), 1767 cm^{-1} (C=O, s); MS (EI): *m/z* calcd for $C_{21}H_{19}N_6O_3$: 403.1518 $[M+H]^+$; found: 403.1515; elemental analysis calcd (%) for $C_{21}H_{18}N_6O_3$: C 62.68, H 4.51, N 20.88; found: C 62.54, H 4.52, N 20.26.

Sonogashira coupling reaction – general procedure: In an oven-dried Schlenk tube, an excess of the alkyne (5 or 6 equiv) was added to a mixture of **1-Br** (1 equiv), CuI (20 mol%), and $[PdCl_2(PPh_3)_2]$ (10 mol%) in DMF and Et_3N. After 2 days of stirring at 70°C and cooling to room temperature, the solvents were removed by cryoscopic transfer. The reaction mixture was extracted with CH_2Cl_2, washed with water, and dried over $MgSO_4$. After filtration and evaporation to dryness, the crude product was purified by column chromatography on silica gel.

1,3,5-Tris{4-[(4-methoxyphenyl)ethynyl]phenyl}-1,3,5-triazinane-2,4,6-trione (2-OMe) from 1-Br: Following the general procedure with **1-Br** (594 mg, 1 mmol), CuI (38 mg, 0.2 mmol), $[PdCl_2(PPh_3)_2]$ (70 mg, 0.1 mmol), DMF (20 mL), Et_3N (5 mL), and 4-ethynylanisole (660 mg, 5 mmol). The product was purified by column chromatography eluting with CH_2Cl_2 (610 mg, 82%).^{1}H NMR (200 MHz, $CDCl_3$, TMS): δ=7.67 (d, $^3J_{H,H}$=8.4 Hz, 6H), 7.52 (d, $^3J_{H,H}$=8.6 Hz, 6H), 7.41 (d, $^3J_{H,H}$=8.4 Hz, 6H), 6.92 (d, $^3J_{H,H}$=8.6 Hz, 6H), 3.87 ppm (s, 9H); $^{13}C\{^1H\}$ NMR (50 MHz, $CDCl_3$, TMS): δ=160.3, 148.7, 133.6, 133.0, 132.8, 128.9, 125.5, 115.2, 114.4, 91.4, 87.5, 55.7 ppm; IR (KBr): $\tilde{\nu}$=2216 (C≡C, m), 1778 (C=O, vw), 1718 cm^{-1} (C=O, s); Raman: $\tilde{\nu}$=2219 (C≡C, m), 1778 cm^{-1} (C=O, vw); HRMS (EI): *m/z* calcd for $C_{48}H_{33}N_3O_6K$: 786.2006 $[M+K]^+$; found: 786.2019; elemental analysis calcd (%) for $C_{48}H_{33}N_3O_6$: C 77.10, H 4.45, N 5.62; found: C 77.16, H 4.47, N 5.57.

2-OMe from 3-H (see later): In an oven-dried Schlenk tube, a solution of **3-H** (150 mg, 0.35 mmol), CuI (5.3 mg, 0.028 mmol), $[PdCl_2(PPh_3)_2]$ (9.8 mg, 0.014 mmol), and 4-iodoanisole (262 mg, 1.12 mmol) in DMF (20 mL) and Et_3N (5 mL) was stirred at 70°C overnight. After cooling to room temperature, the solvents were removed by cryoscopic transfer. The reaction mixture was extracted with CH_2Cl_2, washed with water, and dried over $MgSO_4$. After filtration and evaporation to dryness, the crude product was purified by column chromatography on silica gel with CH_2Cl_2 (100 mg, 38%).

1,3,5-Tris{4-[(4-aminophenyl)ethynyl]phenyl}-1,3,5-triazinane-2,4,6-trione (2-NH$_2$): Following the general procedure with **1-Br** (594 mg, 1 mmol), CuI (38 mg, 0.2 mmol), $[PdCl_2(PPh_3)_2]$ (70 mg, 0.1 mmol), DMF (25 mL), Et_3N (5 mL), and 4-ethynylaniline (585 mg, 5 mmol). The product was purified by column chromatography eluting with a gradient of ethyl acetate/hexane from 2:1 to 4:1 (320 mg, 45%). ^{1}H NMR (200 MHz, CD_3SOCD_3, TMS): δ=7.60 (d, $^3J_{H,H}$=8.4 Hz, 6H), 7.46 (d, $^3J_{H,H}$=8.4 Hz, 6H), 7.24 (d, $^3J_{H,H}$=8.4 Hz, 6H), 6.58 (d, $^3J_{H,H}$=8.4 Hz, 6H), 5.65 ppm (s, 6H); $^{13}C\{^1H\}$ NMR (50 MHz, CD_3SOCD_3, TMS): δ=150.6, 149.5, 134.5, 133.6, 132.2, 130.0, 124.8, 114.4, 108.5, 93.3, 86.7 ppm; IR (KBr): $\tilde{\nu}$=2211 (C≡C, m), 1778 (C=O, vw), 1777 cm^{-1} (C=O, vw); Raman: $\tilde{\nu}$=2208 (C≡ C, m), 1777 cm^{-1} (C=O, vw); HRMS (EI): *m/z* calcd for $C_{45}H_{31}N_6O_3$: 703.2457 $[M+H]^+$; found: 703.2464.

1,3,5-Tris(4-{[4-(dimethylamino)phenyl]ethynyl}phenyl)-1,3,5-triazinane-2,4,6-trione (2-NMe$_2$): Following the general procedure with **1-Br** (300 mg, 0.5 mmol), CuI (19 mg, 0.1 mmol), $[PdCl_2(PPh_3)_2]$ (35 mg, 0.05 mmol), DMF (20 mL), Et_3N (5 mL), and 4-ethynyl-*N*,*N*-dimethylaniline (367 mg, 2.5 mmol). The product was purified by column chromatography with CH_2Cl_2 (200 mg, 50%). ^{1}H NMR (200 MHz, $CDCl_3$, TMS): δ=7.64 (d, $^3J_{H,H}$=8.4 Hz, 6H), 7.45 (d, $^3J_{H,H}$=8.8 Hz, 6H), 7.38 (d, $^3J_{H,H}$=8.4 Hz, 6H), 6.71 (d, $^3J_{H,H}$=8.8 Hz, 6H), 3.03 ppm (s, 18H); $^{13}C\{^1H\}$ NMR (50 MHz, $CDCl_3$, TMS): δ=150.6, 148.7, 133.2, 132.6, 132.5, 128.7, 126.0, 112.2, 109.8, 92.7, 86.9, 40.6 ppm; IR (KBr): $\tilde{\nu}$=2207 (C≡C, m), 1776 (C=O, vw), 1719 cm^{-1} (C=O, s); Raman: $\tilde{\nu}$=2208 (C≡C, m), 1776 cm^{-1} (C=O, vw); HRMS: (EI) *m/z* calcd for $C_{51}H_{43}N_6O_3$: 787.3396 $[M+H]^+$; found: 787.3382; elemental analysis calcd (%) for $C_{51}H_{42}N_6O_3$: C 77.84, H 5.38, N 10.68; found: C 77.27, H 5.48, N 10.07.

1,3,5-Tris(4-{[4-(diphenylamino)phenyl]ethynyl}phenyl)-1,3,5-triazinane-2,4,6-trione (2-NPh$_2$): Following the general procedure with **1-Br** (500 mg, 0.84 mmol), CuI (32 mg, 0.16 mmol), $[PdCl_2(PPh_3)_2]$ (60 mg, 0.08 mmol), DMF (20 mL), Et_3N (5 mL), and 4-ethynyl-*N*,*N*-diphenylaniline (1.13 g, 4.2 mmol). The product was purified by column chromatography with ethyl acetate/hexane 1:4 (600 mg, 61%). ^{1}H NMR (200 MHz, $CDCl_3$, TMS): δ=7.67 (d, $^3J_{H,H}$=8.2 Hz, 6H), 7.43–7.29 (m, 24H), 7.18–7.03 ppm (m, 24H); $^{13}C\{^1H\}$ NMR (50 MHz, $CDCl_3$, TMS): δ=148.7, 147.5, 133.1, 132.7, 129.8, 128.8, 125.5, 124.1, 122.5, 115.8, 91.7, 88.0 ppm (three overlapped peaks); IR (KBr): $\tilde{\nu}$=2209 (C≡C, m), 1772 (C=O, vw), 1718 cm^{-1} (C=O, s); Raman: $\tilde{\nu}$=2216 (C≡C, m), 1777 cm^{-1} (C=O, vw); HRMS (EI): *m/z* calcd for $C_{81}H_{54}N_6O_3$: 1158.4257 $[M]^+$; found: 1158.4235.

1,3,5-Tris{4-[(ferrocenyl)ethynyl]phenyl}-1,3,5-triazinane-2,4,6-trione (5): Following the general procedure with **1-Br** (668 mg, 1.12 mmol), CuI (43 mg, 0.22 mmol), $[PdCl_2(PPh_3)_2]$ (79 mg, 0.11 mmol), DMF (20 mL), Et_3N (5 mL), and ethynylferrocene (1.18 g, 5.6 mmol). The product was purified by column chromatography with CH_2Cl_2 (460 mg, 42%). ^{1}H NMR (200 MHz, $CDCl_3$, TMS): δ=7.64 (d, $^3J_{H,H}$=8.4 Hz, 6H), 7.39 (d, $^3J_{H,H}$=8.4 Hz, 6H), 4.55 (s, 6H), 4.29 ppm (s, 21H); $^{13}C\{^1H\}$ NMR (50 MHz, $CDCl_3$, TMS): δ=148.6, 132.7, 132.6, 128.8, 125.8, 90.7, 85.1, 71.9, 70.4, 69.4, 65.0 ppm; IR (KBr): $\tilde{\nu}$=2205 (C≡C, m), 1777 (C=O, vw), 1710 cm^{-1} (C=O, vs); Raman: $\tilde{\nu}$=2207 (C≡C, vs), 1779 cm^{-1} (C=O, w); HRMS (EI): *m/z* calcd for $C_{57}H_{39}Fe_3N_3O_3$: 981.1039 $[M]^+$; found: 981.1023.

1,3,5-Tris{4-[(trimethylsilyl)ethynyl]phenyl}-1,3,5-triazinane-2,4,6-trione (3-TMS): Following the general procedure with **1-Br** (2 g, 3.37 mmol), CuI (128 mg, 0.67 mmol), $[PdCl_2(PPh_3)_2]$ (236 mg, 0.33 mmol), DMF (50 mL), Et_3N (10 mL), and ethynyltrimethylsilane (2.9 mL, 20.2 mmol). The product was purified by column chromatography with Et_2O/hexane 1:1 (1.37 g, 63%). ^{1}H NMR (200 MHz, $CDCl_3$, TMS): δ=7.61 (d, $^3J_{H,H}$= 8.4 Hz, 6H), 7.35 (d, $^3J_{H,H}$=8.4 Hz, 6H), 0.29 ppm (s, 27H); $^{13}C\{^1H\}$ NMR (50 MHz, $CDCl_3$, TMS): δ=148.5, 133.5, 133.3, 128.8, 125.0, 104.1, 96.6, 0.31 ppm; IR (KBr): $\tilde{\nu}$=2160 (C≡C, m), 1778 (C=O, vw), 1711 cm^{-1} (C=O, vs); Raman: $\tilde{\nu}$=2160 (C≡C, vs), 1781 cm^{-1} (C=O, w); UV/Vis (CH_2Cl_2): λ_{max}(ε) = 254 (84700), 264 (90100), 308 nm (sh, 710 $mol^{-1}dm^3cm^{-1}$); HRMS (EI): *m/z* calcd for $C_{36}H_{39}N_3O_3Si_3$: 645.2299

$[M]^+$; found: 645.2287; elemental analysis calcd (%) for $C_{36}H_{39}N_3O_3Si_3{\cdot}C_4H_8O_2$: C 65.45, H 6.45, N 5.72; found: C 65.23, H 6.63, N 5.72.

1,3,5-Tris(4-ethynylphenyl)-1,3,5-triazinane-2,4,6-trione (3-H): In an oven-dried Schlenk tube, a solution of **3-TMS** (820 mg, 1.27 mmol) and TBAF (0.38 mL, 1 M, 0.38 mmol) in THF (30 mL) was shielded from light and stirred overnight at room temperature. After evacuation of the solvent, the reaction mixture was extracted with CH_2Cl_2, washed with water, and dried over $MgSO_4$. After filtration and evaporation to dryness, the crude product was purified by column chromatography on silica gel with CH_2Cl_2 (300 mg, 55%). ^{1}H NMR (200 MHz, CD_2Cl_2, TMS): $\delta=7.69$ (d, $^3J_{H,H}=8.4$ Hz, 6H), 7.42 (d, $^3J_{H,H}=8.4$ Hz, 6H), 3.29 ppm (s, 3H); ^{13}C{^{1}H} NMR (50 MHz, CD_2Cl_2, TMS): $\delta=148.5$, 134.2, 133.5, 129.0, 123.9, 82.5, 79.1 ppm; IR (KBr): $\tilde{\nu}=3275$ (≡C–H, vs), 2110 (C≡C, w), 1774 (C=O, vw), 1705 cm^{-1} (C=O, vs); Raman: $\tilde{\nu}=2113$ (C≡C, vs), 1774 cm^{-1} (C=O, w); UV/Vis (CH_2Cl_2): $\lambda_{max}(\varepsilon)=251$ (74300), 278 nm (sh, 3500 mol^{-1} dm^3 cm^{-1}); HRMS (EI): *m/z* calcd for $C_{27}H_{15}N_3O_3$: 429.1113 $[M]^+$; found: 429.1105; crystals of X-ray quality were grown by slow diffusion of pentane into a solution of **3-H** in CH_2Cl_2.

Methyl 4-ethynylphenylcarbamate (4): In an oven-dried Schlenk tube, **3-TMS** (467 mg, 0.72 mmol) and potassium carbonate (331 mg, 2.4 mmol) in THF (20 mL) and methanol (20 mL) was stirred at room temperature for 4 h. After evacuation of the solvent, the reaction mixture was extracted with CH_2Cl_2, washed with water, and dried over $MgSO_4$. After filtration and evaporation to dryness, the crude product was purified by column chromatography on silica gel with hexane/Et_2O 1:1 (298 mg, 78%). ^{1}H NMR (200 MHz, $CDCl_3$, TMS): $\delta=7.48$ (d, $^3J_{H,H}=8.6$ Hz, 2H), 7.38 (d, $^3J_{H,H}=8.6$ Hz, 2H), 6.75 (s, 1H), 3.82 (s, 3H), 3.07 ppm (s, 1H); ^{13}C{^{1}H} NMR (50 MHz, $CDCl_3$, TMS): $\delta=154.2$, 138.8, 133.4, 118.6, 117.2, 83.8, 77.0, 52.9 ppm; IR (KBr): $\tilde{\nu}=3330$ (NH, vs), 3279 (≡C–H, vs), 2107 (C≡C, m), 1714 cm^{-1} (C=O, vs); MS (EI): *m/z* calcd for $C_{10}H_9NO_2$: 175.0633 $[M]^+$; found: 175.0629; elemental analysis calcd for $C_{10}H_9NO_2$: C 68.56, H 5.18, N 8.00; found: C 68.64, H 5.29, N 7.73; crystals of X-ray quality were grown by slow diffusion of pentane into a solution of **4** in CH_2Cl_2.

Luminescence measurements: These measurements were performed on dilute solutions contained in 1 cm quartz cells (ca. 10^{-6} M, optical density <0.1) at room temperature (20°C) with an Edinburgh Instruments (FLS920) spectrometer equipped with a 450 W Xenon lamp and a Peltier-cooled Hamamatsu R928P photomultiplier tube in photon-counting mode. Fully corrected emission spectra were obtained at $\lambda_{exc}=\lambda_{max}^{abs}$ with an optical density at $\lambda_{exc}\leq 0.1$ to minimize internal absorption. Luminescence quantum yields were measured according to reported procedures.[52]

TPA measurements: These measurements were conducted by investigating the two-photon excited fluorescence (TPEF) of the fluorophores in CH_2Cl_2 at room temperature (10^{-4} M) according to the experimental protocol established by Xu and Webb.[53] To span the range of $\lambda=700$–980 nm, a Nd:YLF-pumped Ti:sapphire oscillator was used to generate pulses of 150 fs at a rate of 76 MHz. The excitation was focused into the cuvette through a microscope objective (10×, numerical aperture (NA)=0.25). The fluorescence was detected in epifluorescence mode through a dichroic mirror (Chroma 675dcxru) and a barrier filter (Chroma e650sp–2p) by a compact CCD spectrometer module BWTek BTC112E. Total fluorescence intensities were obtained by integrating the corrected emission spectra measured by this spectrometer. TPA cross sections σ_2 were determined from the TPEF cross sections $\sigma_2\Phi$ and the fluorescence quantum yield Φ. TPEF cross sections were measured relative to fluorescein in 0.01 M aqueous NaOH at $\lambda=715$–980 nm,[53–54] using the appropriate solvent-related refractive index corrections.[55] Data points between $\lambda=700$ and 715 nm were corrected according to reference [56]. The quadratic dependence of the fluorescence intensity on the excitation power was checked for each sample and all the wavelengths, thus indicating that the measurements were carried out in intensity regimes at which saturation or photodegradation did not occur.

Computational details: DFT calculations were run using the Gaussian09 package.[57] The standard B3LYP/6–31G* level was retained for all this study based on previous investigations.[39] The reported vibrational frequencies were corrected by using the appropriate scaling factors.[58] In this study, the polarizable continuum model (PCM),[59] including the solvent effect was chosen for the calculation in solution. For the analysis of the molecular-orbital contribution to the electronic absorption bands of the studied compounds, the time-dependent DFT (TDDFT) method was employed and the DFT-optimized ground-state geometries were used. Theoretical absorption spectra were plotted using SWizard,[60] whereas the molecular orbital (MO) analysis was carried out with the AOMix program.[61] DFT calculations were then used to compute the first-order hyperpolarizabilities of selected molecules of this study (see the Supporting Information for more details).[62,63]

X-Ray crystallography: Diffraction data frames for **1-CN**, **1-Br**, **3-H**, and **4** were collected on a APEXII, Bruker-AXS diffractometer using $Mo_{K\alpha}$ radiation ($\lambda=0.71073$ Å). The structures were solved by direct methods with the SIR97 program,[66] and then refined with full-matrix least-square methods based on F^2 (SHELX-97)[67] with the aid of the WINGX[68] program. The contribution of the disordered solvents to the calculated structure factors was estimated following the BYPASS algorithm,[69] implemented as the SQUEEZE option in PLATON.[70] All the non-hydrogen atoms were refined with anisotropic thermal parameters. Hydrogen

Table 6. Crystal data, data collection, and refinement parameters for **1-CN**, **1-Br**, and **3-H** and **4**.

Compound	**1-CN**·C_5H_{12}[a]	**1-Br**	**3-H**·CH_2Cl_2[b]	**4**
formula	$C_{24}H_{12}N_6O_3$	$C_{21}H_{12}Br_3N_3O_3$	$C_{27}H_{15}N_3O_3$	$C_{10}H_9NO_2$
M_r	432.40	594.07	429.42	175.18
T [K]	150(2)	100(2)	100(2)	100(2)
crystal system	orthorhombic	monoclinic	trigonal	monoclinic
space group	*Pcab*	*C*2/*c*	*R*3*c*	*P*21/*a*
a [Å]	12.2308(3)	22.1026(12)	13.5264(13)	9.6420(17)
b [Å]	17.8380(4)	8.3291(4)	13.526	9.5215(16)
c [Å]	20.9795(5)	24.4655(15)	24.608(2)	10.8502(17)
α [°]	90.0	90.0	90.0	90.0
β [°]	90.0	115.842(2)	90.0	115.989(8)
γ [°]	90.0	90.0	120.0	90.0
V [Å^{-3}]	4577.16(19)	4053.6(4)	3899.2(5)	895.4(3)
Z	8	8	6	4
ρ_{calcd} [g cm^{-3}]	1.255	1.947	1.097	1.300
crystal size [mm]	0.49×0.29×0.24	0.55×0.48×0.37	0.25×0.23×0.15	0.55×0.48×0.32
F(000)	1776	2304	1332	368
μ [mm^{-1}]	0.087	6.001	0.073	0.092
hkl	−15/15	−25/28	−16/17	−12/12
	−22/23	−10/10	−17/16	−12/12
	−27/27	−31/31	−25/31	−13/13
total reflections	26228	16577	7587	8995
unique reflections	5200	4646	1002	2040
final R	0.0417	0.0331	0.0693	0.0369
R_w	0.1145	0.0809	0.1716	0.0966
R indices (all data)	0.0519	0.0441	0.0720	0.0392
R_w (all data)	0.1198	0.0862	0.1732	0.0984
S_w	1.096	1.021	1.162	1.070

[a] The highly disordered pentane solvate was suppressed during the structural resolution of this compound by using the SQUEEZE procedure. [b] The highly disordered dichloromethane solvate was suppressed during the structural resolution of this compound by using the SQUEEZE procedure (see the Experimental Section).

atoms were finally included in their calculated positions. A final refinement on F^2 with the unique intensities and 298, 271, 100, or 122 parameters, respectively, converged in each case for the observed reflections with $I > 2\sigma(I)$. The crystallographic data are given in Table 6.

CCDC-843512 (**1CN**), CCDC-843511 (**1Br**), and CCDC-843510 (**4**) contain the supplementary crystallographic data for this paper. These data can be obtained free of charge from The Cambridge Crystallographic Data Centre via www.ccdc.cam.ac.uk/data_request/cif

Acknowledgements

The CNRS is acknowledged for financial support. IDRIS and CINES are acknowledged for an allocation of computer time.

[1] a) R. G. Arnold, J. A. Nelson, J. J. Verbanc, *Chem. Rev.* **1957**, *57*, 47; b) D. K. Hoffmann, *J. Cell. Plast.* **1984**, *20*, 129–137; c) H. Ulrich in *The Chemistry and Technology of Isocyanates*, Wiley, New York, **1996**.

[2] For examples, see the patents cited: a) J.-S. Tang, J. G. Verkade, *Angew. Chem.* **1993**, *105*, 934–936; *Angew. Chem. Int. Ed. Engl.* **1993**, *32*, 896–898; b) J.-S. Tang, J. G. Verkade, *J. Org. Chem.* **1994**, *59*, 4931–4938; c) J. Yang, J. G. Verkade, *J. Am. Chem. Soc.* **1998**, *120*, 6834–6835; d) S. R. Foley, Y. Zhou, G. P. A. Yap, D. S. Richeson, *Inorg. Chem.* **2000**, *39*, 924–929; e) S. R. Foley, G. P. A. Yap, D. S. Richeson, *Organometallics* **1999**, *18*, 4700–4705; f) M. Roman, B. Andrioletti, M. Lemaire, J.-M. Bernard, J. Schwartz, P. Barbeau, *Tetrahedron* **2011**, *67*, 1506–1510; g) H. A. Duong, M. J. Cross, J. Louie, *Org. Lett.* **2004**, *6*, 4679–4681.

[3] H. Ulrich, *J. Cell. Plast.* **1981**, *17*, 31–34.

[4] Z. Bukac, J. Sebenda, *J. Chem. Prum.* **1985**, *35*, 361–363, and references therein.

[5] a) A. K. Zhitinkina, N. A. Shibanova, O. G. Tarakhanov, *Russ. Chem. Rev.* **1985**, *54*, 1104; b) F. Paul, S. Moulin, O. Piechaczyk, P. Le Floch, J. A. Osborn, *J. Am. Chem. Soc.* **2007**, *129*, 7294–7304; c) Z. Puzstai, G. Vlad, A. Bodor, I. T. Horvath, H. J. Laas, R. Halpaap, F. U. Richter, *Angew. Chem.* **2006**, *118*, 113–116; *Angew. Chem. Int. Ed.* **2006**, *45*, 107–110, and references therein.

[6] F. Hettche, R. W. Hoffmann, *New J. Chem.* **2003**, *27*, 172–177.

[7] A. P. Murray, M. J. Miller, *J. Org. Chem.* **2003**, *68*, 191–194.

[8] O. Olkhovyk, M. Jaroniec, *J. Am. Chem. Soc.* **2005**, *127*, 60–61.

[9] V. R. Thalladi, S. Brasselet, D. Bläser, R. Boese, J. Zyss, A. Nangia, G. R. Desiraju, *Chem. Commun.* **1997**, 1841–1842.

[10] a) O. Maury, H. Le Bozec, *Acc. Chem. Res.* **2005**, *38*, 691–703; b) J. J. Wolff, R. Wortmann, *J. Prakt. Chem.* **1998**, *340*, 99–111; c) J. Zyss, I. Ledoux, *Chem. Rev.* **1994**, *94*, 77–105.

[11] a) F. Terenziani, C. Katan, E. Badaeva, S. Tretiak, M. Blanchard-Desce, *Adv. Mater.* **2008**, *20*, 4641–4678; b) G. S. He, L.-S. Tan, Q. Zheng, P. N. Prasad, *Chem. Rev.* **2008**, *108*, 1245–1330; c) B. R. Cho, K. H. Son, S. H. Lee, Y.-S. Song, Y.-K. Lee, S.-J. Jeon, J. H. Choi, H. Lee, M. Cho, *J. Am. Chem. Soc.* **2001**, *123*, 10039–10045; d) W. H. Lee, S. H. Lee, J.-A. Kim, J. H. Choi, M. Cho, S.-J. Jeon, B. R. Cho, *J. Am. Chem. Soc.* **2001**, *123*, 10658–10667.

[12] For examples, see: a) S.-H. Lee, J.-R. Park, M.-Y. Jeong, H. M. Kim, S. Li, J. Song, S. Ham, S.-J. Jeon, B. R. Cho, *ChemPhysChem* **2006**, *7*, 206–212; b) M. J. Piao, K. Chajara, S. J. Yoon, H. M. Kim, S.-J. Jeon, H. M. Kim, K. Song, I. Asselberghs, A. Persoons, K. Clays, B. R. Cho, *J. Mater. Chem.* **2006**, *16*, 2273–2281; c) B. Traber, J. J. Wolff, F. Rominger, T. Oeser, R. Gleiter, M. Goebel, R. Wortmann, *Chem. Eur. J.* **2004**, *10*, 1227–1238; d) J. Brunel, O. Mongin, A. Jutand, I. Ledoux, J. Zyss, M. Blanchard-Desce, *Chem. Mater.* **2003**, *15*, 4139–4148; e) J. J. Wolff, F. Siegler, R. Matschiner, R. Wortmann, *Angew. Chem.* **2000**, *112*, 1494–1498; *Angew. Chem. Int. Ed.* **2000**, *39*, 1436–1439; f) R. Wortmann, C. Glania, P. Krämer, R. Matschiner, J. J. Wolff, S. Kraft, B. Treptow, E. Barbu, D. Längle, G. Görlitz, *Chem. Eur. J.* **1997**, *3*, 1765–1773.

[13] H. M. Kim, B. R. Cho, *J. Mater. Chem.* **2009**, *19*, 7402–7409.

[14] G. Argouarch, R. Veillard, T. Roisnel, A. Amar, A. Boucekkine, A. Singh, I. Ledoux, F. Paul, *New J. Chem.* **2011**, *35*, 2409–2411.

[15] a) M. G. Dekamin, K. Vamira, M. Farahmand, S. Sagheb-Asl, Z. Karimi, *Catal. Commun.* **2010**, *12*, 226–230; b) S. M. Raders, J. G. Verkade, *J. Org. Chem.* **2010**, *75*, 5308–5311; c) H.-X. Li, M.-L. Cheng, H.-M. Wang, X.-J. Yang, Z.-G. Ren, J.-P. Lang, *Organometallics* **2011**, *30*, 208–214; d) H.-M. Wang, H.-X. Li, X.-Y. Yu, Z.-G. Ren, J.-P. Lang, *Tetrahedron* **2011**, *67*, 1530–1535.

[16] Y. Nambu, T. Endo, *J. Org. Chem.* **1993**, *58*, 1932–1934.

[17] For a recent account on many of the **1-X** derivatives, see references [15a, b, d]; earlier and more specific reports on these compounds also exist (X = NO_2, Me, and OMe; references [18, 2e], respectively).

[18] a) Y. Li, H. Matsuma, M. Yamanaka, T. Takahashi, *Tetrahedron* **2004**, *60*, 1393–1400; b) A. Zhou, L. Cao, H. Li, Z. Liu, H. Cho, W. P. Henry, C. U. Pittman, Jr., *Tetrahedron Lett.* **2006**, *62*, 4188–4200.

[19] K. Nakamoto in *Infrared spectra of inorganic and coordination compounds*, 2nd ed., Wiley-Interscience, New York, **1970**.

[20] G. Grelaud, M. P. Cifuentes, T. Schwich, G. Argouarch, S. Petrie, R. Stranger, F. Paul, M. G. Humphrey, *Eur. J. Inorg. Chem.* **2012**, 65–75.

[21] a) O. Akira, S. Hiroyoshi, I. Tsutomu, T. Hayashi, M. Tsutami, I. Koji, K. Tadash, U. Keiji, I. Yuji, N. Ryousuke, Patent WO03035407 (A1), Mitsui Chemical, Japan, **2003**; b) I. Tsutomu, S. Hiroyoki, O. Akira, JP 2004249635A, Mitsui Chemical, Japan, **2004**, pp. 1–41.

[22] F. H. Allen, O. Kennard, D. G. Watson, L. Brammer, A. G. Orpen, R. Taylor, *J. Chem. Soc. Perkin Trans.*, **1987**, S1–S19.

[23] Y. Wu, S. Wang, X. Zhu, G. Yang, Y. Wei, L. Zhang, H.-B. Song, *Inorg. Chem.* **2008**, *47*, 5503–5511.

[24] L. M. Yagupolskii, S. V. Shelyazhenko, I. I. Maletina, V. N. Petrik, E. B. Rusanov, A. N. Chernega, *Eur. J. Org. Chem.* **2001**, 1225–1233.

[25] Y.-P. Luoa, H.-B. Zhou, *Acta Crystallogr. E* **2006**, *62*, o538–o539.

[26] X. Zhu, J. Fan, Y. Wu, S. Wang, L. Zhang, G. Yang, Y. Wei, C. Yin, H. Zhu, S. Wu, H. Zhang, *Organometallics* **2009**, *28*, 3882–3888.

[27] For published crystallographic data on other **1-X** derivatives, see for instance: a) Y. G. Gololobov, P. V. Petrovskii, E. M. Ivanova, O. A. Linchenko, R. Schutzler, L. Ernst, P. G. Jones, A. Karacar, M. Freytag, S. Okucu, *Russ. Chem. Bull.* **2003**, *52*, 427–436; b) A. A. Yartseva, L. S. Koldrov, S. S. Galibeev, V. P. Arkhireev, N. I. Naumkina, I. A. Litvinov, A. T. Gubaidullin, *J. Struct. Chem.* **2007**, *48*, 1138–1144.

[28] a) G. R. Desiraju, *Acc. Chem. Res.* **1991**, *24*, 290–296; b) G. R. Desiraju, *Acc. Chem. Res.* **1996**, *29*, 441–449.

[29] A complex vibronic fine structure for **2-OMe** is also apparent on the lowest-energy band, but not for the other **2-X** congeners; likewise, a vibronic fine structure was apparent on the most-intense band of compound **3-H**; these vibronic progressions are apparently complex and cannot be attributed to a single vibrational mode.

[30] a) L. Cuffe, R. D. A. Hudson, J. F. Gallagher, S. Jennings, C. J. McAdam, R. B. T. Connelly, A. R. Manning, B. H. Robinson, J. Simpson, *Organometallics* **2005**, *24*, 2051–2060; b) C. Engtrakul, L. R. Sita, *Nanoletters* **2001**, *1*, 541–549; c) S. Barlow, S. R. Marder, *Chem. Commun.* **2000**, 1555–1562.

[31] C. Hansch, A. Leo, R. W. Taft, *Chem. Rev.* **1991**, *91*, 165–195.

[32] J.-P. Sauvage, J.-P. Colin, J.-C. Chambron, S. Guillerez, C. Coudret, *Chem. Rev.* **1994**, *94*, 993–1019.

[33] Note that a significant solvatochromism has sometimes been evidenced for other octopular derivatives in spite of the absence of dipole moment in the ground state; see references [12d, 34].

[34] Y. Luo, *J. Am. Chem. Soc.* **1998**, *120*, 11188–11189.

[35] a) E. Lippert, *Z. Naturforsch. A* **1955**, *10*, 541–545; b) N. Mataga, Y. Kaifu, M. Koizumi, *Bull. Chem. Soc. Jpn.* **1955**, *28*, 690–691.

[36] a) L. Porrès, O. Mongin, C. Katan, M. Charlot, T. Pons, J. Mertz, M. Blanchard-Desce, *Org. Lett.* **2004**, *6*, 47–50; b) C. Le Droumaguet, O. Mongin, M. H. V. Werts, M. Blanchard-Desce, *Chem. Commun.* **2005**, 2802–2804; c) M. Parent, O. Mongin, K. Kamada, C. Katan, M. Blanchard-Desce, *Chem. Commun.* **2005**, 2029–2031.

[37] a) P. R. Bangal, D. M. K. Lam, L. A. Peteanu, M. J. Van der Auweraer, *J. Phys. Chem. B* **2004**, *108*, 16834–16840; b) C. Katan, F. Terenziani, O. Mongin, M. H. V. Werts, L. Porrès, T. Pons, J. Mertz, S. Tretiak, M. Blanchard-Desce, *J. Phys. Chem. A* **2005**, *109*, 3024–3037; c) R. Stahl, C. Lambert, C. Kaiser, R. Wortmann, R. Jakober, *Chem. Eur. J.* **2006**, *12*, 2358–2370; d) F. Terenziani, C. Le Droumaguet, C. Katan, O. Mongin, M. Blanchard-Desce, *ChemPhysChem* **2007**, *8*, 723–734.
[38] a) M. Charlot, L. Porrès, C. D. Entwistle, A. Beeby, T. B. Marder, M. Blanchard-Desce, *Phys. Chem. Chem. Phys.* **2005**, *7*, 600–606; b) J. C. Collings, S.-Y. Poon, C. Le Droumaguet, M. Charlot, C. Katan, L.-O. Pålsson, A. Beeby, J. A. Mosely, H. M. Kaiser, D. Kaufmann, W.-Y. Wong, M. Blanchard-Desce, T. B. Marder, *Chem. Eur. J.* **2009**, *15*, 198–208; c) H. M. Kim, B. R. Cho, *Chem. Commun.* **2009**, 153–164.
[39] F. Ibersiene, D. Hammoutène, A. Boucekkine, C. Katan, M. Blanchard-Desce, *J. Mol. Struct.* **2008**, *866*, 58–62.
[40] A. Willetts, J. E. Rice, D. M. Burland, D. P. Shelton, *J. Chem. Phys.* **1992**, *97*, 7590–7599.
[41] D. Beljonne, W. Wenseleers, E. Zojer, Z. Shuai, H. Vogel, S. J. K. Pond, J. W. Perry, S. R. Marder, J.-L. Brédas, *Adv. Funct. Mater.* **2002**, *9*, 631–641.
[42] S. J. Stickler, R. A. Berg, *J. Chem. Phys.* **1962**, *37*, 814–822.
[43] E. Hendrickx, K. Clays, A. Persoons, *Acc. Chem. Res.* **1998**, *31*, 675–683.
[44] See for instance: a) B. Kirtman, J. M. Luis, *J. Chem. Phys.* **1998**, *108*, 10008–10012; b) B. Champagne, *Chem. Phys. Lett.* **1996**, *261*, 57–65. Such effects are however believed to be weak in absence of static field: c) L. Adamowicz, R. J. Bartlett, *J. Phys. Chem.* **1986**, *84*, 4988–4991; d) H. Sekino, R. J. Bartlett, *J. Phys. Chem.* **1986**, *84*, 2726–2733.
[45] F. Terenziani, C. Sissa, A. Painelli, *J. Phys. Chem. B* **2008**, *112*, 5079–5087.
[46] C. Katan, O. Mongin, G. Alcaraz, M. Vaultier, A. Boucekkine, M. Blanchard-Desce, *Proc. SPIE - Int. Soc. Opt. Eng.* **2004**, *26*, 5517–5528.
[47] G. Alcaraz, L. Euzenat, O. Mongin, C. Katan, I. Ledoux, J. Zyss, M. Blanchard-Desce, M. Vaultier, *Chem. Commun.* **2003**, 2766–2767.
[48] B. Y. Lee, G. C. Bazan, *J. Am. Chem. Soc.* **2000**, *122*, 8577–8578.
[49] O. Mongin, L. Porres, C. Katan, T. Pons, J. Mertz, M. Blanchard-Desce, *Tetrahedron Lett.* **2003**, *44*, 8121–8125.
[50] Y. Z. Cui, Q. Fang, G. Xue, G. B. Xu, L. Yin, W. T. Yu, *Chem. Lett.* **2005**, *34*, 644–645.
[51] O. Mongin, L. Porrès, M. Charlot, C. Katan, M. Blanchard-Desce, *Chem. Eur. J.* **2007**, *13*, 1481–1498.
[52] a) G. R. Eaton, *Pure Appl. Chem.* **1988**, *60*, 1107–1114; b) N. Demas, G. A. Crosby, *J. Phys. Chem.* **1971**, *75*, 991–1024.
[53] C. Xu, W. W. Webb, *J. Opt. Soc. Am. B* **1996**, *13*, 481–491.
[54] M. A. Albota, C. Xu, W. W. Webb, *Appl. Opt.* **1998**, *37*, 7352–7356.
[55] M. H. V. Werts, N. Nerambourg, D. Pélégry, Y. Le Grand, M. Blanchard-Desce, *Photochem. Photobiol. Sci.* **2005**, *4*, 531–538.
[56] C. Katan, S. Tretiak, M. H. V. Werts, A. J. Bain, R. J. Marsh, N. Leonczek, N. Nicolaou, E. Badaeva, O. Mongin, M. Blanchard-Desce, *J. Phys. Chem. B* **2007**, *111*, 9468–9483.
[57] M. J. Frisch, G. W. Trucks, H. B. Schlegel, G. E. Scuseria, M. A. Robb, J. R. Cheeseman, G. Scalmani, V. Barone, B. Mennucci, G. A. Petersson, H. Nakatsuji, M. Caricato, X. Li, H. P. Hratchian, A. F. Izmaylov, J. Bloino, G. Zheng, J. L. Sonnenberg, M. Hada, M. Ehara, K. Toyota, R. Fukuda, J. Hasegawa, M. Ishida, T. Nakajima et al., Gaussian, Inc., Wallingford CT, **2009**.
[58] J. P. Merrick, D. Moran, L. Radom, *J. Phys. Chem. A* **2007**, *111*, 11683–11700.
[59] a) S. Miertus, E. Scrocco, J. Tomasi, *Chem. Phys.* **1981**, *55*, 117–119; b) C. Amovilli, V. Barone, R. Cammi, E. Cancès, M. Cossi, B. Mennucci, C. S. Pomelli, J. Tomasi, *Adv. Quant. Chem.* **1998**, *32*, 227–262.
[60] S. Gorelsky, revision 4.2. ed., available from: http://www.sg-chem.net/.
[61] S. Gorelsky, available from: http://www.sg-chem.net/.
[62] D. A. Kleinman, *Phys. Rev.* **1977**, *126*, 1977–1979.
[63] J. Zyss, *J. Chem. Phys.* **1993**, *98*, 6583–6599.
[64] M. J. S. Dewar, E. G. Zoebisch, E. F. Healy, J. J. P. Stewart, *J. Am. Chem. Soc.* **1985**, *107*, 3902–3909.
[65] a) J. J. P. Stewart, *Int. J. Quant. Chem.* **1996**, *58*, 133–146; b) J. J. P. Stewart, *MOPAC Program*, ed., Fujitsu Ltd, Tokyo, **1997**.
[66] A. Altomare, M. C. Burla, M. Camalli, G. Cascarano, C. Giacovazzo, A. Guagliardi, A. G. G. Moliterni, G. Polidori, R. Spagna, *J. Appl. Crystallogr.* **1999**, *32*, 115–119.
[67] G. M. Sheldrick, SHELX97-2, Program for the refinement of crystal structures, University of Göttingen (Germany), **1997**.
[68] L. J. Farrugia, *J. Appl. Crystallogr.* **1999**, *32*, 837–838.
[69] P. van.der Sluis, A. L. Spek, *Acta Crystallogr. Sect. A* **1990**, *46*, 194–201.
[70] A. L. Spek, *Appl. Crystallogr.* **2003**, *36*, 7–13.

Received: February 14, 2012
Published online: July 24, 2012

